High expression of insulin-like growth factor binding protein-3 is correlated with lower portal invasion and better prognosis in human hepatocellular carcinoma

Shinichi Aishima,[1,*] Yuji Basaki,[1,4,8,*] Yoshinao Oda,[1] Yousuke Kuroda,[1] Yunosuke Nishihara,[1] Kenichi Taguchi,[5] Akinobu Taketomi,[2] Yoshihiko Maehara,[2] Fumihito Hosoi,[4,6] Yuichiro Maruyama,[4,6] Abbas Fotovati,[6] Shinji Oie,[4] Mayumi Ono,[3,4,6] Takato Ueno,[6] Michio Sata,[6] Hirohisa Yano,[6,7] Masamichi Kojiro,[6,7] Michihiko Kuwano[4,6] and Masazumi Tsuneyoshi[1]

Departments of [1]Anatomic Pathology, [2]Surgery and Science, and [3]Medical Biochemistry, Graduate School of Medical Sciences, Kyushu University, Fukuoka 812-8582; [4]Station-II for Collaborative Research, Kyushu University, Fukuoka 812-8582; [5]Kyushu National Cancer Center, Fukuoka 811-1395; [6]Research Center for Innovative Cancer Therapy, Kurume University, Kurume 830-0011; [7]Department of Pathology, Kurume University School of Medicine, Kurume 830-0011, Japan

(Received April 19, 2006/Revised July 24, 2006/Accepted July 26, 2006/Online publication September 15, 2006)

Insulin-like growth factor binding protein-3 (IGFBP-3) modulates cell proliferation of various cancer cell types. However, it remains unclear how IGF–IGFBP-3-signaling is involved in growth and progression of hepatocellular carcinoma (HCC). The aim of the present study was to evaluate the role of IGFBP-3 in HCC. Type 1 receptor for IGF (IGF-1R) was expressed at various levels in the seven lines examined, but IGF-2R was not expressed. Of the seven lines, the growth of HAK-1B, KIM-1, KYN-2 and HepG2 cells was stimulated in a dose-dependent manner by the exogenous addition of IGF-I or IGF-II, but the HAK-1A, KYN-1 and KYN-3 cell lines showed no growth. Exogenous addition of IGFBP-3 markedly blocked IGF-I and IGF-II-stimulated cell growth of KYN-2 and HepG2 cells, and moderately stimulated that of KIM-1 and HAK-1B cells, but no growth of the KYN-1, KYN-3 and HAK-1A cell lines was observed. IGF-I enhanced the phosphorylation of IGF-1R, Akt and Erk1/2 in KYN-2 cells, and coadministration of IGFBP-3 blocked all types of activation by IGF-I investigated here. In contrast, no such activation by IGF-I was detected in KYN-3 cells. IGFBP-3 also suppressed IGF-I-induced cell invasion by KYN-2 cells. Moreover, we were able to observe the apparent expression of IGFBP-3 in KYN-3 cells, but not in the other six cell lines. Furthermore reduced expression of IGFBP-3, but not that of IGF-1R, was significantly correlated with tumor size, histological differentiation, capsular invasion and portal venous invasion. Low expression of IGFBP-3 was independently associated with poor survival. IGFBP-3 could be a molecular target of intrinsic importance for further development of novel therapeutic strategy against HCC. (*Cancer Sci* 2006; 97: 1182–1190)

Hepatocellular carcinoma (HCC) is one of the most common and aggressive malignant tumors worldwide. The long-term prognosis of HCC patients has remained unsatisfactory due to the high incidence of intrahepatic recurrence, which depends on portal venous invasion and the high incidence of intrahepatic metastasis, as well as multicentric development of new tumors.[1,2] Moreover, our understanding of the molecular mechanisms underlying the progression of HCC and the development of effective therapeutic targets remain to be studied in further detail.

One candidate among the many growth factors that are closely associated with growth of HCC cells is insulin-like growth factor (IGF).[3] The biological effects of IGF are mediated via type 1 IGF receptor (IGF-1R), which leads to activation of the mitogen-activated protein kinase (MAPK) signaling pathway involved in cell growth and metabolism.[4,5] Mutation of another type 2 receptor (M6P/IGF-2R) and upregulation of IGF-II are expected to be responsible for the early stages of human hepatocarcinogenesis.[6,7] However, it remains unclear how the IGF system is involved in the progression of HCC. IGF are known to bind to IGF binding proteins (IGFBP), which regulate activity and function of IGF.[8] IGFBP-3 is the most abundant IGFBP that is present in non-cancerous liver tissues and serves as a negative regulator of cell proliferation in human HCC.[9–12] IGFBP-3 is also known to regulate cell growth independently of its effects on IGF-stimulated growth in other types of malignancy.[13–16]

In our present study, we investigated how IGFBP-3 exerts its antiproliferative effects on HCC cell lines in culture, and using immunohistochemical analyses we further examined whether or not the expression of IGFBP-3 in human clinical samples is associated with the clinicopathological characteristics of HCC. We discuss plausible roles of IGFBP-3 in the IGF-dependent and -independent cell proliferation of HCC, and also the clinical significance of IGFBP-3 in patients with HCC.

Materials and Methods

Cell culture and reagents. HAK-1A, HAK-1B, KIM-1, KYN-1, KYN-2 and KYN-3 were established at Kurume University (Kurume, Japan) as described previously.[17–21] HepG2 was purchased from American Type Culture Collection (Manassas, VA, USA). These cell lines were grown in Dulbecco's modified Eagle's medium (DMEM) supplemented with 10% fetal bovine serum. Human IGF-I (hIGF-I), hIGF-II and hIGFBP-3 were purchased from R&D systems (Minneapolis, MN, USA). Anti-IGF-1Rα, antiphospho-IGF-1R, anti-IRS-1, anti-PKB/Akt, antiphospho-PKB/Akt, anti-Erk and antiphospho-Erk were obtained from Cell Signaling (Beverly, MA, USA). Anti-IGFBP-3 was from Santa Cruz (Santa Cruz, CA, USA). Anti-glyceraldehyde-3-phosphate dehydrogenase (GAPDH) was purchased from TREVIGEN (Gaithersburg, MD, USA).

Western blotting. Western blotting was carried out as described previously.[22] Briefly, cells were lysed in a lysis buffer (pH 7.4) containing 20 mM Tris-HCl, 1% Triton X-100, 50 mM each of NaCl and NaF, 5 mM ethylenediaminetetraacetic acid, 1 mM Na_3VO_4, 1 mM phenylmethylsulfonylfluoride and 10 μg/mL each of aprotinin and leupeptin. The lysates were separated by sodium dodecylsulfate–polyacrylamide gel electrophoresis, and then transferred to a nitrocellulose membrane.

Small interfering RNA transfection. The small interfering RNA (siRNA) corresponding to nucleotide sequences of IGF-1R (5′-GCAUCGAACUCCUCUUCUCAGUUAA-3′) and IGFBP-3 (5′-AAUCAUCAUCAAGAAAGGGCAUU-3′)[23] were purchased

[8]To whom correspondence should be addressed. E-mail: yubasaki@yahoo.co.jp
*S. Aishima and Y. Basaki contributed equally to this work.

doi: 10.1111/j.1349-7006.2006.00322.x

from Invitrogen (Carlsbad, CA, USA) and QIAGEN (Valencia, CA, USA), respectively. A negative control siRNA was obtained from Invitrogen. siRNA duplexes were transfected using Lipofectamine 2000 and Opti-MEM medium (Invitrogen) according to the manufacturer's recommendations.

Real-time quantitative polymerase chain reaction. The extraction of total RNA was carried out using TRIsol solution (Life Technologies, Grand Island, NY, USA). Real-time quantitative polymerase chain reaction (PCR) was carried out using the Real-Time PCR system 7300 (Applied Biosystems, Foster City, CA, USA) as described previously.[24] In brief, the PCR amplification reaction mixtures (20 μL) contained cDNA, primer pairs, dual-labeled fluorogenic probe and TaqMan Universal PCR Master Mix. The primer pairs and probe were obtained from Applied Biosystems. The relative gene expression for each sample was determined using the formula:

$$2^{-\Delta Ct} = 2^{Ct(GAPDH)-Ct(IGF\text{-}1R)},$$

which reflected the IGF-1R gene expression normalized to GAPDH levels.

Cell proliferation assay. Aliquots of medium containing 3.0×10^3 cells were seeded into a 96-well plate. The following day, the medium was replaced with serum-free DMEM medium with or without IGF. The plate was then treated for 72 h before the addition of WST-8 (2-[2-methocy-4-nitrophenyl]-3-[4-nitrophenyl]-5-[2,4-disulfophenyl]-2H-tertrazolium) and absorbance recorded at 450 nm.

Quantification of IGFBP-3 in conditioned medium. The concentration of IGFBP-3 in conditioned medium from the HCC cell lines was measured using a commercially available enzyme-linked immunosorbent assay (ELISA) kit (R&D systems). The cells were suspended at a density of 3.0×10^3 cells/mL in 48-well plates and the suspensions were then cultured for 16 h. The supernatant was replaced with fresh medium after 24 h.

Matrigel invasion assay. This assay carried out as described previously.[25] In brief, BD BioCoat Matrigel Invasion Chambers (BD Bioscience, Bedford, MA, USA) were used according to the manufacturer's instructions. KYN-2 cells (1×10^5) in serum-free DMEM containing 0.1% bovine serum albumin were seeded onto Matrigel-coated filters in the upper chambers. In the lower chambers, DMEM medium with or without IGF-I was added as a chemoattractant. After 24 h of incubation, cells on the upper surface of the filters were removed with a cotton swab, and the filters were fixed with 100% methanol and stained with Giemsa dye. The cells that had invaded to the lower side of the filters were viewed under a microscope and counted in five fields of view. The invasive ability of the cancer cells was expressed as the mean number of cells in five fields. The assay was carried out as three independent experiments.

Patients and samples. We reviewed the clinical data and surgically resected tissue from 87 consecutive patients who underwent hepatectomy for primary HCC without preoperative treatment between 1992 and 2000. Written informed consent was obtained from each patient before tissue acquisition. The study was approved by the Human Investigation Committee at the Kyushu University School of Medicine (Fukuoka, Japan). All specimens were obtained from files at the Department of Anatomic Pathology at Kyushu University. All tumors were defined as HCC, and the pathological features were determined histologically based on the classification of the Liver Cancer Study Group of Japan.[26]

For measurement of serum IGF-I and IGFBP-3 levels, 92 subjects with HCC were included (age, 45–83 years; median, 67.6 years; male/female, 64/28; hepatitis B virus antigen (HBsAg) positive, 16; hepatitis C virus antibody (HCV-Ab) positive, 68; and HBsAg/HCV-Ab negative, 8). The diagnosis was based on ultrasonography, contrast-enhanced computed tomography, magnetic resonance imaging angiography and histological findings. All patients underwent hepatectomy for primary HCC without preoperative treatment at the Kurume University Hospital.

Immunohistochemistry. The tissue sections (4 μm) were stained with anti-IGFBP-3, anti-IGF-1Rα or antiphospho-IGF-1R. A biotinylated secondary antibody was then applied and incubated with peroxidase-conjugated streptavidin, chromogenized by diaminobenzidine. The staining was evaluated semiquantitatively in the selected HCC components containing a predominant histological grade and the results were compared with those in adjacent, non-neoplastic hepatocytes. The staining for IGFBP-3 was divided into low (less than 10% of tumor cells are positive) and high (more than 10% of tumor cells are positive) expression groups according to the percentage of immunoreactive cells. The evaluation for IGF-1R was dependent on its intensity when IGFBP-3 was evaluated by counting immunoreactive cells.

Statistical analysis. Differences in cell number, the levels of proteins and serum IGF-I and IGFBP-3 levels being examined were analyzed using the Mann–Whitney *U*-test. The correlation between serum IGF-I and IGFBP-3 levels and degree of HCC progression, and between immunohistochemical results and clinicopathological factors, were evaluated using the χ^2-test, Fisher's exact test and Mann–Whitney *U*-test. Overall survival was measured from the time of surgery until death with disease, or until the end of follow up. Patients who died of causes unrelated to the disease were censored at the time of death ($n = 3$). One patient was lost from follow up at 2 months after surgery. Survival curves were calculated using the Kaplan–Meier method, and the differences between the curves were analyzed using the log-rank test. Cox's proportional hazard model with a stepwise procedure was used for the multivariate survival analysis. The results were considered significant if the *P*-value was less than 0.05.

Results

IGF-dependent cell growth in some HCC cell lines. IGF-1R, IRS-1, Akt and Erk were expressed at various levels among the seven cell lines, although no IGF-2R expression was detected (Fig. 1A). Both IGF-I and IGF-II stimulated cell proliferation of HAK-1B, KIM-1, KYN-2 and HepG2 in a dose-dependent manner. Moreover, IGF-I and IGF-II stimulated only slight, if any, cell growth among HAK-1A, KYN-1 and KYN-3 (Fig. 1B). IGF-I effectively stimulated cell proliferation of KYN-2 much more than IGF-II did, but both factors showed similar stimulatory effects on growth of HAK-1B, KIM-1 and HepG2 cells.

We next examined whether or not IGF-dependent cell growth of HCC cells is mediated through IGF-1R. The transfection of IGF-1R siRNA in KYN-2 cells led to a downregulation of IGF-1R expression in a dose-dependent manner (Fig. 1C). The growth of KYN-2 cells increased to approximately 1.5-fold the size of untreated controls when treated with IGF, and this IGF-dependent stimulation of growth was almost completely blocked by 40–100 nM IGF-1R siRNA (Fig. 1D).

Effect of IGFBP-3 on IGF-induced cell growth. The effect of IGFBP-3 on IGF-induced cell growth was examined. The IGF-dependent cell growth of KYN-2 and HepG2 was almost completely blocked by treatment with IGFBP-3 at 1–10 μg/mL, whereas that of HAK-1B and KIM-1 was significantly blocked by treatment with 10 μg/mL IGFBP-3. In contrast, the growth of HAK-1 A, KYN-1 and KYN-3 cells was not at all inhibited by treatment with IGFBP-3 (Fig. 2A). Next we carried out an ELISA assay in order to determine whether or not HCC cell lines produce IGFBP-3. Of the seven cell lines examined here, we were able to observe unequivocal production of higher amounts of IGFBP-3 in the KYN-3 cells, but this was not the case in the other cell lines (Fig. 2B).

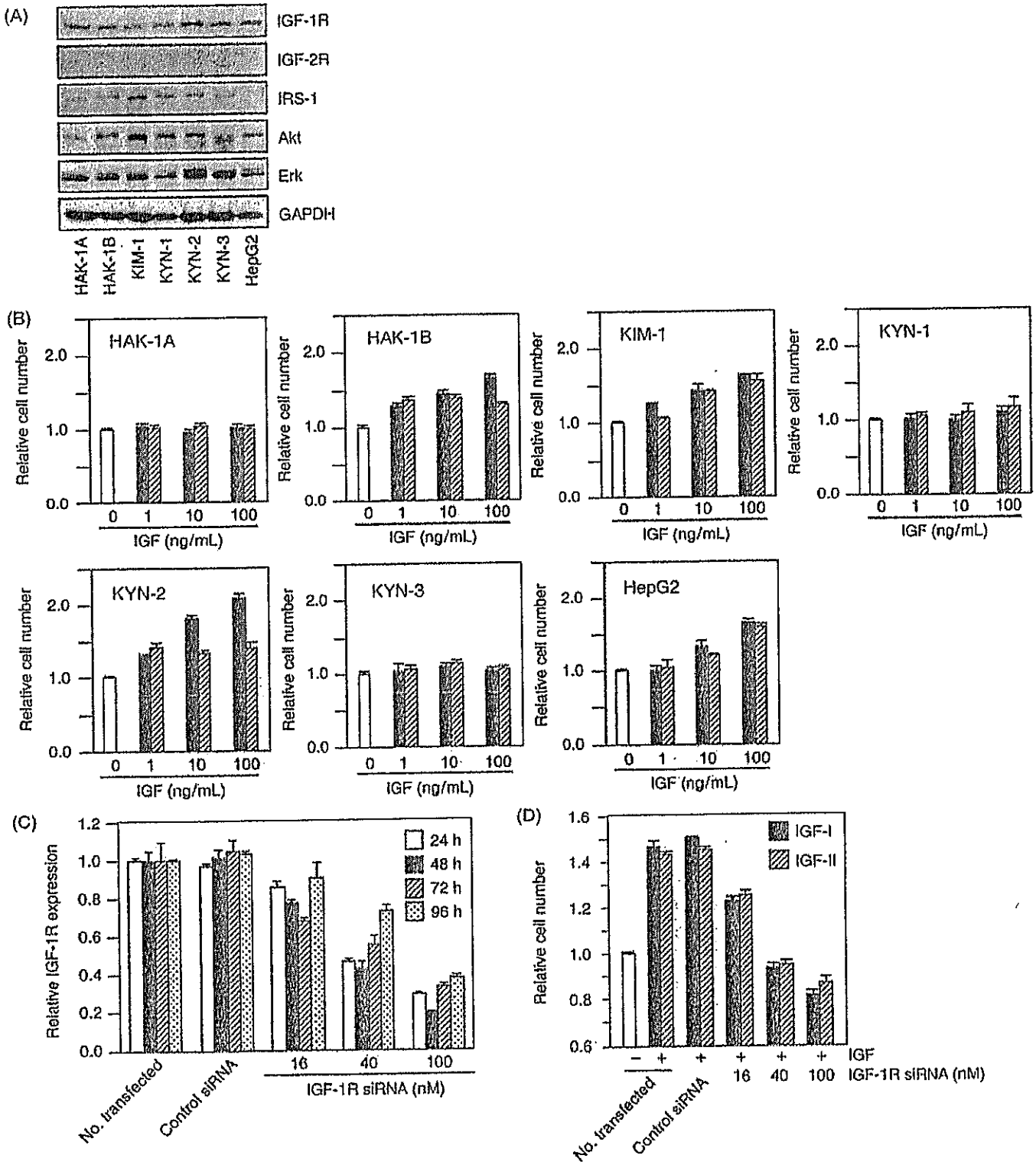

Fig. 1. (A) Expression of type 1 insulin-like growth factor (IGF) receptor (IGF-1R), IGF-2R, IRS-1, Akt and Erk was determined by immunoblotting conducted on protein lysates extracted from these cell lines. The detection of glyceraldehyde-3-phosphate dehydrogenase (GAPDH) served as a loading control. (B) Effects of IGF-I and IGF-II on the proliferation of seven hepatocellular carcinoma cell lines. The cells were treated with or without IGF at concentrations of 1, 10 or 100 ng/mL for 72 h in serum-free media, and then colorimetric WST assays were carried out. Each bar represents IGF-I (closed bar) or IGF-II (hatched bar). The data are expressed as the mean ± SD. (C) Inhibition by IGF-1R small interfering RNA (siRNA) treatment of IGF-1R gene expression of KYN-2 cells. KYN-2 cells were transfected with IGF-1R siRNA at concentrations of 0, 16, 40 and 100 nM, and the cells were incubated for the periods of time indicated. After incubation, total RNA was extracted and gene silencing was analyzed by real-time quantitative polymerase chain reaction. (D) Effect of IGF-1R siRNA on the proliferation of IGF-I (closed bar) or IGF-II (hatched bar)-stimulated KYN-2 cells. The cells were stimulated with 100 ng/mL of IGF-I or IGF-II after 24 h of siRNA treatment, and a WST assay was carried out 72 h after IGF stimulation. The data are expressed as the mean ± SD.

doi: 10.1111/j.1349-7006.2006.00322.x

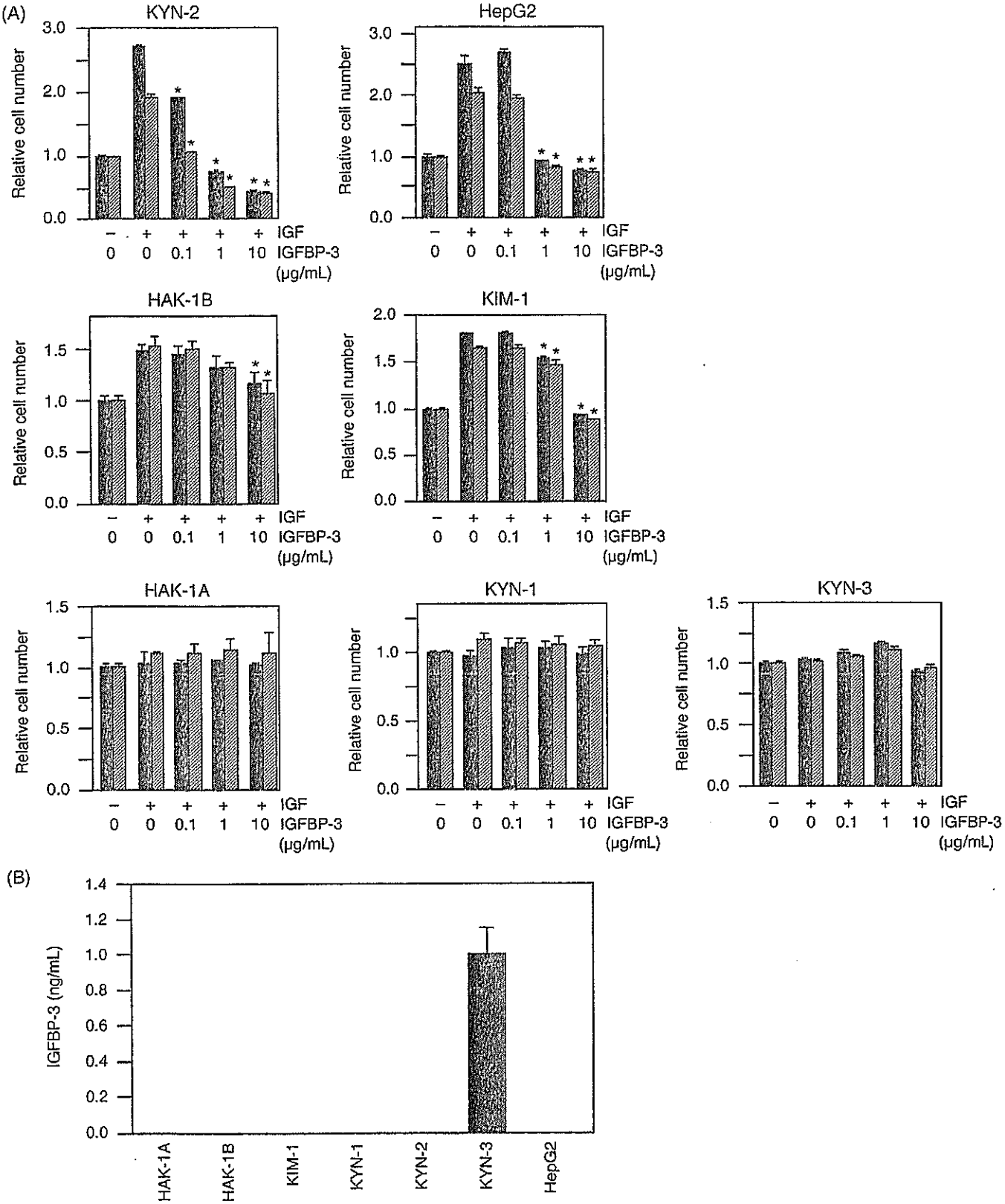

Fig. 2. (A) The effects of insulin-like growth factor (IGF) binding protein (IGFBP)-3 on IGF-I- or IGF-II-dependent cell proliferation of seven hepatocellular carcinoma cell lines. The cells were incubated with either serum-free medium, 100 ng/mL of IGF-I (closed bar) or 100 ng/mL of IGF-II (hatched bar) in the presence of various concentrations of IGFBP-3 for 72 h. After incubation, colorimetric WST assays were carried out. *Significant differences ($P < 0.01$) compared with treatment with IGF alone in the absence of IGFBP-3. The data are expressed as the mean ± SD. (B) Cellular production of IGFBP-3 in KYN-3 cells. IGFBP-3 protein levels in the culture medium with the seven cell lines examined here were assayed quantitatively with enzyme-linked immunosorbent assay systems. The data are the average of triplicate wells ± SD.

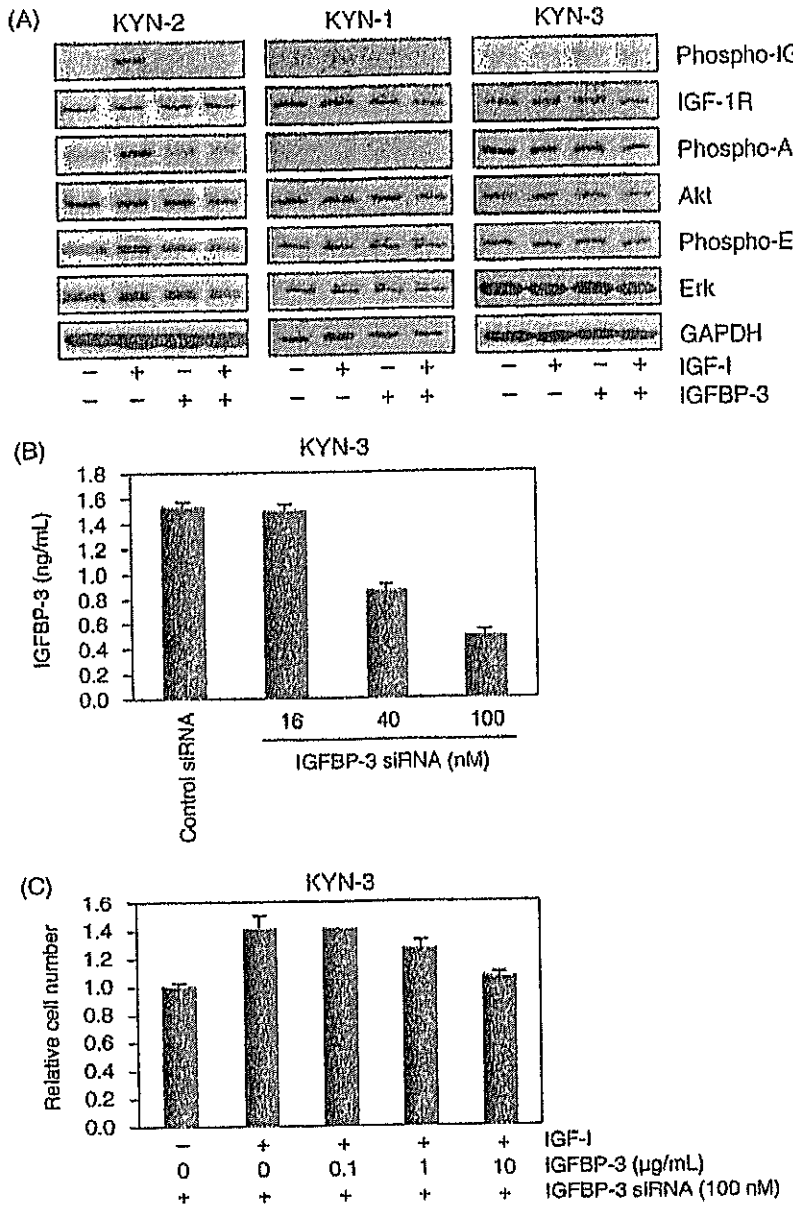

Fig. 3. (A) Effects of insulin-like growth factor (IGF)-I and IGF binding protein (IGFBP)-3 on the phosphorylation of type 1 IGF receptor (IGF-1R), Akt and Erk in KYN-2, KYN-1 and KYN-3 cells. Serum-deprived cells were treated with 100 ng/mL IGF-I and/or with 10 μg/mL IGFBP-3 for 10 min. Cell lysates were blotted with the antibodies indicated. The detection of glyceraldehyde-3-phosphate dehydrogenase (GAPDH) served as a loading control. (B) Inhibition by IGFBP-3 small interfering RNA (siRNA) treatment of IGFBP-3 expression in KYN-3 cells. KYN-3 cells were transfected with IGFBP-3 siRNA at concentrations of 0, 16, 40 and 100 nM, and the cells were incubated for 24 h. After incubation, IGFBP-3 protein levels in the culture medium were assayed quantitatively with enzyme-linked immunosorbent assay systems. The data are the average of triplicate wells ± SD. (C) Restoration of IGF-I-stimulated proliferation of KYN-3 cells by IGFBP-3 siRNA. KYN-3 cells were treated for 24 h with 100 nM IGFBP-3 siRNA and further incubation with 100 ng/mL of IGF-I in the absence or presence of various doses of IGFBP-3 for 72 h. The data are expressed as the mean ± SD.

Effect of IGFBP-3 on IGF-dependent signaling, cell growth and invasion. We further examined whether the activation of IGF-1R and its downstream signaling were modulated by IGFBP-3 in three cell lines: KYN-2 with IGF-dependent cell growth, and KYN-1 and KYN-3 with IGF-independent cell growth. Treatment with IGF-I markedly enhanced phosphorylation of IGF-1R, with concomitant phosphorylation of both Akt and Erk in KYN-2 cells, but such effects were not observed in KYN-1 and KYN-3 cells (Fig. 3A). The IGF-I-induced phosphorylation of IGF-1R, Akt and Erk was almost completely inhibited in KYN-2 by coadministration of IGFBP-3.

Cell growth of KYN-3 was not stimulated by IGF and not blocked by coadministration of IGFBP-3: KYN-3 cells produced a significant amount of IGFBP-3 (Fig. 2). We next examined whether production of IGFBP-3 by KYN-3 cells could be responsible for their reduced response to IGF. The transfection of IGFBP-3 siRNA in KYN-3 cells led to a knock-down of IGFBP-3 expression in a concentration-dependent manner (Fig. 3B). Cell growth of KYN-3 was found to be increased to approximately 1.4-fold over the untreated controls by IGF-I when treated with 100 nM IGFBP-3 siRNA (Fig. 3C). This IGF-I-dependent growth stimulation was significantly inhibited by 10 μg/mL IGFBP-3 in IGFBP-3 siRNA-treated KYN-3 cells (Fig. 3A,C).

Insulin-like growth factor-I plays an important role in invasion and migration of various malignant cell types including melanoma and pancreatic carcinoma.[27,28] We next examined whether IGFBP-3 could affect the invasive ability of IGF-stimulated KYN-2 cells by Matrigel invasion assay. Invaded cells were increased to approximately 9.0-fold of untreated controls when treated with 1000 ng/mL IGF-I (Fig. 4). In addition, the IGF-I-induced cell invasion was significantly suppressed by 52% by treatment with 100 μg/mL IGFBP-3 (Fig. 4). Thus, IGFBP-3 could inhibit both invasion and cell proliferation induced by IGF in HCC.

Expression of IGFBP-3 and IGF-1R and their clinicopathological implications in clinical HCC. The expression of IGF-1R and IGFBP-3 was determined in human HCC samples by

doi: 10.1111/j.1349-7006.2006.00322.x

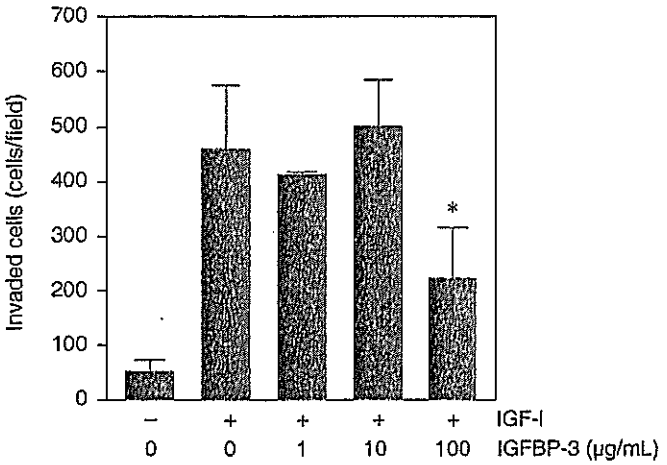

Fig. 4. Effect of insulin-like growth factor (IGF) binding protein (IGFBP)-3 on invasion by IGF-stimulated KYN-2 cells in Matrigel invasion assay. Serum-deprived KYN-2 cells (1×10^5) were seeded onto Matrigel-coated filters in the upper chambers, and Dulbecco's modified Eagle's medium with or without IGF-I (1000 ng/mL) in the presence of various concentrations of IGFBP-3. The cell invasiveness was quantified as the mean cell number in five fields of view per filter. Columns, mean of three independent experiments; bars, ±SD.

immunohistochemical analysis. The clinicopathological characteristics of 87 HCC patients, from whom the clinical samples were derived, are shown in Table 1. A representative immunohistochemical data of case 1 of well-differentiated HCC is shown in Fig. 5A: the expression of both IGFBP-3 and IGF-1R protein was higher in carcinoma tissue than in adjacent hepatocytes (Fig. 5). In contrast, a representative case of poorly differentiated HCC (case 2 in Fig. 5A) exhibited reduced expression of both IGFBP-3 and IGF-1R in carcinoma cells, compared with that in adjacent hepatocytes (Fig. 5A,d–f). In non-cancerous tissue of case 2, IGF-1R and IGFBP-3 were found to be expressed in hepatocytes, but not in stromal cells such as inflammatory cells, Kupffer cells and endothelial cells (data not shown). Table 2 gives a summary of the immunohistochemical analysis of IGFBP-3 and IGF-1R expression in 87 clinical specimens. The immunohistochemical analysis of IGF-1R and IGFBP-3 expression in HCC samples revealed that the intensity of staining in carcinoma was similar to or stronger than that of adjacent hepatocytes in 57 cases of IGFBP-3 and 58 cases of IGF-1R (Table 2).

We then determined whether or not the expression of IGFBP-3 and IGF-1R was associated with clinicopathological features of clinical HCC samples. However, we were unable to obtain any statistically significant results regarding IGF-1R expression and clinicopathological parameters. In contrast, a close association between IGFBP-3 expression and certain clinicopathological characteristics was observed (Table 2). Low expression of IGFBP-3 was observed in cases with larger tumor size, poorly differentiated histology, capsular invasion and portal venous invasion. Moreover, IGF-1R expression was found to correlate positively with IGFBP-3 expression.

Univariate and multivariate survival analysis. The overall survival of patients with low IGFBP-3 expression was significantly worse than those with high IGFBP-3 expression (Fig. 5B). In the univariate postoperative survival analysis, tumor size, histological differentiation, portal vein invasion, TNM classification and intrahepatic metastasis were also associated with poor survival (data not shown). The multivariate survival analysis revealed that TNM classification (stage 3/4), low IGFBP-3 expression and larger tumor size (>4 cm) were independent prognostic factors (Table 3).

Table 1. Clinicopathological characteristics of 87 patients

Characteristic	*n*
Sex	
Male	67
Female	20
Age (years)	36–83 (mean: 62.3)
Tumor size (cm)	0.8–14.5 (mean: 3.9)
Virus marker	
HBV*	13 (14.9%)
HCV*	60 (69.0%)
HBV* and HCV*	4 (0.5%)
Liver cirrhosis	37 (42.5%)
TNM stage	
I	12
II	31
III	19
IV	15
Histological differentiation	
Well	11
Moderate	54
Poor	22
Capsular invasion	56 (64.4%)
Portal venous invasion	40 (46.0%)
Intrahepatic metastasis	29 (33.3%)

HBV*, positive for hepatitis B virus antigen; HCV*, positive for hepatitis C virus antibody.

Serum IGF-I and IGFBP-3 levels in patients with HCC. Finally, we examined whether serum levels of IGFBP-3 or IGF-I were associated with HCC staging in 92 patients. Serum mean levels of IGF-I and IGFBP-3 in the stage I, II, III and IV groups were 92.1 ± 35.2 and 1.36 ± 0.34, 99.6 ± 37.4 and 1.30 ± 0.35, 74.6 ± 27.1 and 1.02 ± 0.30, and 91.7 ± 58.0 and 1.35 ± 1.10, respectively. There were negative correlations between staging of HCC and serum IGF-I levels (Fig. 6A) or serum IGFBP-3 levels (Fig. 6B). However, no statistically significant difference was observed in the correlation between HCC staging and serum IGF-I levels or serum IGFBP-3 levels.

Discussion

In the present study, we classified seven HCC cell lines into two groups that exhibited IGF-dependent (HAK-1B, KIM-1, KYN-2 and HepG2) and independent (HAK-1A, KYN-1 and KYN-3) growth, whereby all seven cell lines expressed various levels of IGF-1R. The growth of the former four cell lines was susceptible to the inhibitory effects of IGFBP-3, whereas the growth of the latter three cells lines did not show such susceptibility. IGF-1R, Akt and Erk were markedly activated in response to IGF-I in KYN-2 cells with IGF-dependent growth and invasion, and their activities were almost completely blocked by coadministration of IGFBP-3. In contrast, IGF-I did not activate IGF-1R, Akt or Erk in KYN-3 cells exhibiting IGF-independent growth, and IGFBP-3 was unable to block phosphorylation of these molecules. Relevant studies have shown that the growth of HepG2 cells was inhibited by coadministration of IGFBP-3,[9,12] which is consistent with our present data regarding HepG2 cells. These findings suggest that IGFBP-3 inhibits both growth and invasion of HCC cells through its interaction with IGF.

Of these seven cell lines, only KYN-3 produced significant amounts of IGFBP-3. The cellular levels of IGF-1R in the KYN-3 cells were similar to those in KYN-2 cells, which were also highly sensitive to IGFBP-3-induced growth inhibition. The constitutive expression of IGFBP-3 might interfere

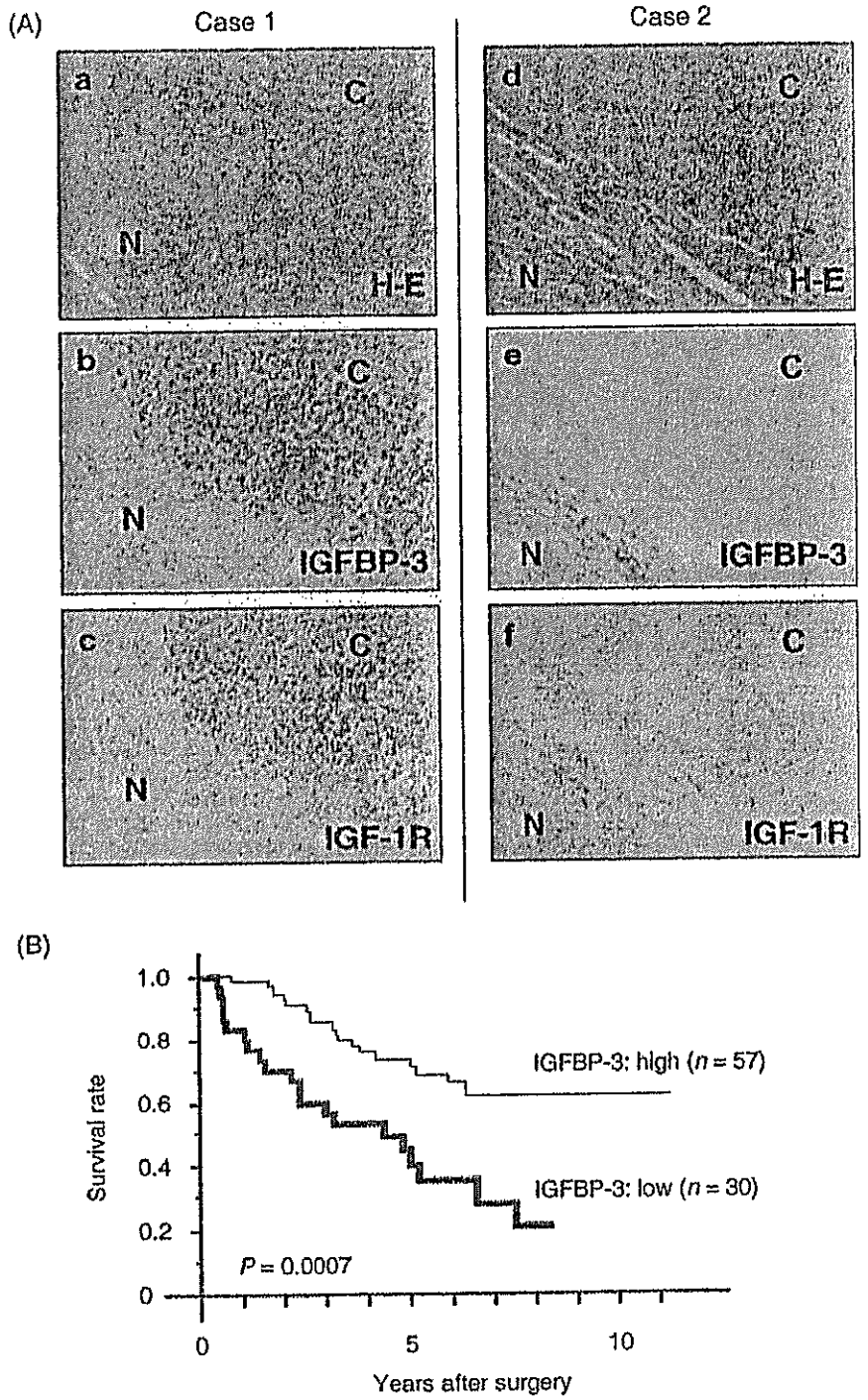

Fig. 5. (A) Immunohistochemical expression of insulin-like growth factor (IGF) binding protein (IGFBP)-3 in hepatocellular carcinoma (HCC). Two representative cases of well-differentiated HCC (case 1) and poorly differentiated HCC (case 2). The expression of both IGFBP-3 and type 1 IGF receptor (IGF-1R) was stronger in the HCC than in the adjacent liver in the cases of well-differentiated HCC (b,c). In contrast, cases of poorly differentiated HCC showed reduced expression of IGFBP-3 and IGF-1R in the HCC tissue compared with that of the adjacent liver tissue (e,f). (a,d) Hematoxylin–eosin (H-E) staining. C, cancerous region; N, non-cancerous region. (B) The overall survival of patients with low IGFBP-3 expression was significantly worse than that of patients with high IGFBP-3 expression ($P = 0.0007$).

with IGF-1R-dependent growth signaling in KYN-3 cells, resulting in lowered susceptibility to growth inhibition by the exogenous addition of IGFBP-3. Reduced expression of IGFBP-3 by treatment with siRNA could restore IGF-I-dependent cell growth in KYN-3 cells. The IGF-1R in KYN-3 cells might be occupied with endogenous IGFBP-3, thus resulting in a lack of further inhibition by exogenous IGFBP-3.

However, the growth of KYN-1 and HAK-1A was not stimulated by exogenous addition of these IGF, and was also insensitive to growth inhibition by IGFBP-3 when both cell lines expressed cellular levels of IGF-1R comparable to those in KYN-3 and KYN-2. Unlike the KYN-3 cells, neither the KYN-1 nor the HAK-1A cells produced significant amounts of IGFBP-3. It remains unclear why IGFBP-3 was unable to block the proliferation of these two cell lines, HAK-1 A and KYN-1, both of which express IGF-1R. Although IGF can activate IGF-1R as well as Akt and Erk, in KYN-2, KIM-1, HAK-1B and HepG2, all of which exhibit IGF-dependent cell growth, these IGF were unable to activate IGF-1R and its downstream signaling pathways in HAK-1A and KYN-1 cells, and in KYN-3 cells, all of which exhibit IGF-independent cell growth. It is possible that IGF-1R in the HAK-1A and KYN-1 cell lines

doi: 10.1111/j.1349-7006.2006.00322.x

Table 2. Correlation of clinicopathological features and type 1 insulin-like growth factor (IGF) receptor (IGF-1R) or IGF binding protein (IGFBP)-3 protein expression in hepatocellular carcinoma

Variable	IGF-1R			IGFBP-3		
	High (n = 58)	Low (n = 29)	P-value	High (n = 57)	Low (n = 30)	P-value
Mean age (years)	62.5	61.9	0.7397	63.2	60.6	0.1827
Male : female	45 : 13	22 : 7	0.8570	45 : 12	22 : 8	0.5542
Mean tumor size (cm)	3.6	4.6	0.1337	3.0	5.7	<0.0001
Liver cirrhosis	25 (43.1%)	12 (41.4%)	0.8781	26 (45.6%)	11 (36.7%)	0.4223
Stage						
I/II	31	12	0.2885	31	12	0.2021
III/IV	27	17		26	18	
Histological differentiation						
Well/moderate/poor	9/38/10	2/16/12	0.0557	11/38/8	0/16/14	0.0007
Capsular invasion	37 (63.8%)	19 (65.5%)	0.8742	31 (54.3%)	25 (83.3%)	0.0074
Portal venous invasion	26 (44.8%)	14 (48.3%)	0.7610	17 (29.8%)	23 (76.7%)	<0.0001
Intrahepatic metastasis	19 (32.8%)	10 (34.5%)	0.8722	19 (33.3%)	10 (33.3%)	>0.9999
High IGF-1R expression	–	–		45 (77.6%)	13 (43.3%)	0.0008

Table 3. Significant variables determined by multivariable survival analysis

Variables	Coefficient	SE	Coefficient/SE	P-value
Stage III/IV	0.988	0.353	2.797	0.0052
IGFBP-3	0.841	0.329	2.558	0.0105
Tumor size (>4 cm)	0.670	0.332	2.015	0.0440

IGFBP, insulin-like growth factor binding protein.

might be functionally inactive. There appeared to be no mutations in either the transmembrane domain or in the tyrosine kinase domain of IGF-1R in any of the HCC cell lines used in the present study (data not shown). Further studies should be carried out in order to gain a better understanding of the mechanism by which IGFBP-3 exerts its inhibitory effects on the growth of these HCC cell lines.

Thirty-nine percent of HCC clinical samples have been found to exhibit lower levels of IGF-1R than does non-neoplastic adjacent liver tissue.[12] Consistent with the results of that previous study, our immunohistochemical analysis of 87 HCC samples demonstrated lower levels of IGF-1R expression in approximately 40% of the human HCC tissue samples investigated, compared with matched, non-tumorous tissue samples. The expression of IGF-1R in HCC was not found to be significantly associated with any of a number of clinicopathological characteristics. However, to our surprise, high levels of IGF-1R expression were significantly associated with high levels of IGFBP-3 expression in HCC. Higher levels of IGF-1R expression might modulate the expression of IGFBP-3 in cases of HCC, but this possibility will require further investigation.

Immunohistochemical analysis of the expression of IGFBP-3 in cancerous and non-cancerous lesions in cases of HCC further demonstrated a close correlation of high or low IGFBP-3 expression with tumor size, histological differentiation and portal venous invasion, but not with intrahepatic metastasis. The close association of tumor size and differentiation in HCC with the expression of IGFBP-3 suggests that IGFBP-3 might play a key role in tumor growth and progression in HCC. The malignant characteristics of HCC are partly due to their metastatic potential via intrahepatic metastasis and portal venous invasion. Of these two types of metastatic potential in cases of HCC, the expression of IGFBP-3 was found to be more specifically correlated with portal venous invasion than with intrahepatic metastasis, thus suggesting the role of IGFBP-3 in portal venous invasion. However, there appeared no significant correlation of HCC staging with serum levels of IGFBP-3 or serum levels of IGF-I when 92 HCC patients were analyzed. Our present clinical data with determination of serum IGFBP-3 levels are also consistent with previous relevant studies.[11,29] Further study should be carried out in order to determine the potential role of IGFBP-3 in the above-mentioned malignant characteristics associated with HCC.

In conclusion, the absence or presence of IGFBP-3 expression and a functional IGF-1R could affect the state of IGF-dependent cell growth in HCC cell lines in culture. The expression of

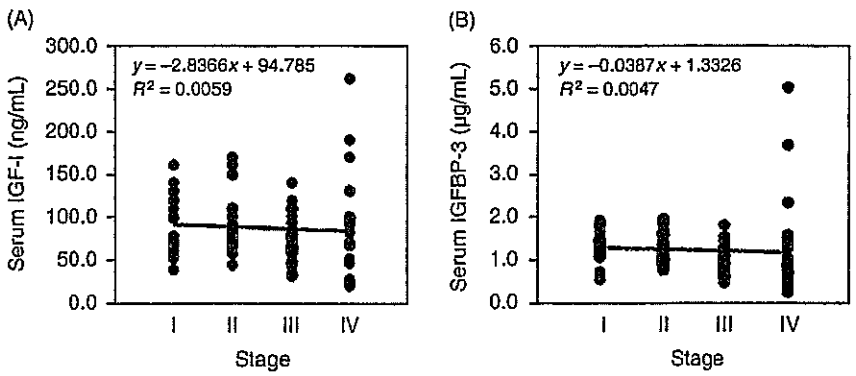

Fig. 6. Correlation between hepatocellular carcinoma (HCC) staging and serum insulin-like growth factor (IGF)-I levels or serum IGF binding protein (IGFBP)-3 levels in patients with HCC (n = 92). (A) Correlation between HCC staging and serum IGF-I levels. (B) correlation between HCC staging and serum IGFBP-3 levels. Patients of stage I (n = 22), II (n = 17), III (n = 31) and IV (n = 22).

IGFBP-3 was also significantly correlated with histological differentiation, tumor size, portal venous invasion and prognosis, but not with intrahepatic metastasis in the HCC studied here. As IGFBP-3 plays a pivotal role in tumor enlargement and metastasis in HCC, it should be considered as a possible molecular target for the development of novel therapeutic strategies used in the treatment of HCC.

Acknowledgments

This study was supported in part by Health and Labour Sciences Research Grants of Third Term Comprehensive Control Research for Cancer from the Ministry of Health, Labour and Welfare. We would like to thank Drs Yuji Yamada and Tadafumi Terada (Taiho Pharmaceutical Co., Hanno, Japan) for fruitful discussions of this study.

References

1 Shimada M, Takenaka K, Gion T *et al.* Prognosis of recurrent hepatocellular carcinoma: a 10-year surgical experience in Japan. *Gastroenterology* 1996; **111**: 720–6.
2 Adachi E, Maehara S, Tsujita E *et al.* Clinicopathologic risk factors for recurrence after a curative hepatic resection for hepatocellular carcinoma. *Surgery* 2002; **131**: 148–52.
3 Scharf JG, Schmidt-Sandte W, Pahernik SA, Ramadori G, Braulke T, Hartmann H. Characterization of the insulin-like growth factor axis in a human hepatoma cell line (PLC). *Carcinogenesis* 1998; **19**: 2121–8.
4 LeRoith D, Werner H, Beitner-Johnson D, Roberts CT Jr. Molecular and cellular aspects of the insulin-like growth factor I receptor. *Endocr Rev* 1995; **16**: 143–63.
5 Ito T, Sasaki Y, Wands JR. Overexpression of human insulin receptor substrate 1 induces cellular transformation with activation of mitogen-activated protein kinases. *Mol Cell Biol* 1996; **16**: 943–51.
6 Oka Y, Waterland RA, Killian JK *et al.* M6P/IGF2R tumor suppressor gene mutated in hepatocellular carcinomas in Japan. *Hepatology* 2002; **35**: 1153–63.
7 Sedlaczek N, Hasilik A, Neuhaus P, Schuppan D, Herbst H. Focal overexpression of insulin-like growth factor 2 by hepatocytes and cholangiocytes in viral liver cirrhosis. *Br J Cancer* 2003; **88**: 733–9.
8 Khandwala HM, McCutcheon IE, Flyvbjerg A, Friend KE. The effects of insulin-like growth factors on tumorigenesis and neoplastic growth. *Endocr Rev* 2000; **21**: 215–44.
9 Hanafusa T, Yumoto Y, Nouso K *et al.* Reduced expression of insulin-like growth factor binding protein-3 and its promoter hypermethylation in human hepatocellular carcinoma. *Cancer Lett* 2002; **176**: 149–58.
10 Gong Y, Cui L, Minuk GY. The expression of insulin-like growth factor binding proteins in human hepatocellular carcinoma. *Mol Cell Biochem* 2000; **207**: 101–4.
11 Mattera D, Capuano G, Colao A *et al.* Increased IGF-I : IGFBP-3 ratio in patients with hepatocellular carcinoma. *Clin Endocrinol* 2003; **59**: 699–706.
12 Huynh H, Chow PK, Ooi LL, Soo KC. A possible role for insulin-like growth factor-binding protein-3 autocrine/paracrine loops in controlling hepatocellular carcinoma cell proliferation. *Cell Growth Differ* 2002; **13**: 115–22.
13 Oh Y, Muller HL, Lamson G, Rosenfeld RG. Insulin-like growth factor (IGF)-independent action of IGF-binding protein-3 in Hs578T human breast cancer cells: Cell surface binding and growth inhibition. *J Biol Chem* 1993; **268**: 14 964–71.
14 Rajah R, Valentinis B, Coehn P. Insulin-like growth factor (IGF)-binding protein-3 induces apoptosis and mediates the effects of transforming growth factor-1 on programmed cell death through a p53 and IGF-independent mechanism. *J Biol Chem* 1997; **272**: 12 181–8.
15 Gill ZP, Perks CM, Newcomb PV, Holly JM. Insulin-like growth factor-binding protein (IGFBP-3) predisposes breast cancer cells to programmed cell death in a non-IGF-dependent manner. *J Biol Chem* 1997; **272**: 25 602–7.
16 Kim HS, Ingermann AR, Tsubaki J, Twigg SM, Walker GE, Oh Y. Insulin-like growth factor-binding protein 3 induces caspase-dependent apoptosis through a death receptor-mediated pathway in MCF-7 human breast cancer cells. *Cancer Res* 2004; **64**: 2229–37.
17 Murakami T. Establishment and characterization of human hepatocellular carcinoma cell line (KIM-1). *Acta Hepathol Jpn* 1984; **25**: 532–9.
18 Murakami T, Maruiwa M, Fukuda K, Kojiro M, Tanaka M, Tanikawa K. Characterization of a new human hepatoma cell line (KYN-3) derived from the ascites of the hepatoma patient. *Jpn J Cancer Res* 1988; Proceedings of the Japanese Cancer Association: 292 [Abstract].
19 Yano H, Kojiro M, Nakashita T. A new human hepatocellular carcinoma cell line (KYN-1) with a transformation to adenocarcinoma *in vitro*. *Cell Dev Biol* 1986; **22**: 637–46.
20 Yano H, Maruiwa M, Murakami T *et al.* A new human pleomorphic hepatocellular carcinoma cell line, KYN-2. *Acta Pathol Jpn* 1988; **38**: 953–66.
21 Yano H, Iemura A, Fukuda K, Mizoguchi A, Haramaki M, Kojiro M. Establishment of two distinct human hepatocellular carcinoma cell lines from a single nodule showing clonal dedifferentiation of cancer cells. *Hepatology* 1993; **18**: 320–7.
22 Basaki Y, Ikizawa K, Kajiwara K, Yanagihara Y. CD40-mediated tumor necrosis factor receptor-associated factor 3 signaling upregulates IL-4-induced germline Cepsilon transcription in a human B cell line. *Arch Biochem Biophys* 2002; **405**: 199–204.
23 Stewart LV, Weigel NL. Role of insulin-like growth factor binding proteins in 1α,25-dihydroxyvitamin D (3)-induced growth inhibition of human prostate cancer cells. *Prostate* 2005; **64**: 9–19.
24 Kaneko Y, Kitazato K, Basaki Y. Integrin-linked kinase regulates vascular morphogenesis induced by vascular endothelial growth factor. *J Cell Sci* 2004; **117**: 407–15.
25 Maruyama Y, Ono M, Kawahara A *et al.* Tumor growth suppression in pancreatic cancer by a putative metastasis suppressor gene Cap43/NDRG1/drg-1 through modulation of angiogenesis. *Cancer Res* 2006; **66**: 6233–42.
26 Liver Cancer Study Group. *The General Rules for the Clinical and Pathological Study of Primary Liver Cancer*, 4th edn. Tokyo: Kanehara Publications, 2000.
27 Stracke M, Engel J, Wilson L, Rechler M, Liotta L, Schiffmann E. The type I insulin-like growth factor receptor is a motility receptor in human melanoma cells. *J Biol Chem* 1989; **264**: 21 544–9.
28 Brooks P, Klemke R, Schon S, Lewis J, Schwartz M, Cheresh D. Insulin-like growth factor receptor cooperates with integrin αvβ5 to promote tumor cell dissemination *in vivo*. *J Clin Invest* 1997; **99**: 1390–8.
29 Unsal E, Koksal D, Yurdakul AS, Atikcan S, Cinaz P. Analysis of insulin like growth factor 1 and insulin like growth factor binding protein 3 levels in bronchoalveolar lavage fluid and serum of patients with lung cancer. *Respir Med* 2005; **99**: 559–65.

doi: 10.1111/j.1349-7006.2006.00322.x

Novel SN-38–Incorporating Polymeric Micelles, NK012, Eradicate Vascular Endothelial Growth Factor–Secreting Bulky Tumors

Fumiaki Koizumi,[1] Masayuki Kitagawa,[2] Takahito Negishi,[1] Takeshi Onda,[2] Shin-ichi Matsumoto,[2] Tetsuya Hamaguchi,[3] and Yasuhiro Matsumura[1]

[1]Investigative Treatment Division, Research Center for Innovative Oncology, National Cancer Center Hospital East, Kashiwa, Chiba, Japan; [2]Pharmaceutical Research Laboratories, Research and Development Group, Nippon Kayaku Co., Ltd, Kita-ku, Tokyo, Japan; and [3]Department of Medicine, National Cancer Center Hospital, Tyuo-ku, Tokyo, Japan

Abstract

7-Ethyl-10-hydroxy-camptothecin (SN-38), a biological active metabolite of irinotecan hydrochloride (CPT-11), has potent antitumor activity but has not been used clinically because it is a water-insoluble drug. For delivery by i.v. injection, we have successfully developed NK012, a SN-38-releasing nanodevice. The purpose of this study is to investigate the pharmacologic character of NK012 as an anticancer agent, especially in a vascular endothelial growth factor (VEGF)–secreting tumor model. The particle size of NK012 was ~20 nm with a narrow size distribution. NK012 exhibited a much higher cytotoxic effect against lung and colon cancer cell lines as compared with CPT-11. NK012 showed significantly potent antitumor activity against a human colorectal cancer HT-29 xenograft as compared with CPT-11. Enhanced and prolonged distribution of free SN-38 in the tumor was observed after the injection of NK012. NK012 also had significant antitumor activity against bulky SBC-3/Neo (1,533.1 ± 1,204.7 mm^3) and SBC-3/VEGF tumors (1,620.7 ± 834.0 mm^3) compared with CPT-11. Furthermore, NK012 eradicated bulky SBC-3/VEGF tumors in all mice but did not eradicate SBC-3/Neo tumors. In the drug distribution analysis, an increased accumulation of SN-38 in SBC-3/VEGF tumors was observed as compared with that in SBC-3/Neo tumors. NK012 markedly enhanced the antitumor activity of SN-38, especially in highly VEGF-secreting tumors, and could be a promising SN-38-based formulation. (Cancer Res 2006; 66(20): 10048-56)

Introduction

The antitumor plant alkaloid camptothecin (CPT) is a broad-spectrum anticancer agent that targets DNA topoisomerase I. Although CPT has shown promising antitumor activity *in vitro* and *in vivo* (1, 2), it has not been clinically used because of its low therapeutic efficacy and severe toxicity (3, 4). Among CPT analogues, irinotecan hydrochloride (CPT-11) has recently been shown to be active against colorectal, lung, and ovarian cancer (5–9). CPT-11 itself is a prodrug and is converted to 7-ethyl-10-hydroxy-CPT (SN-38), a biologically active metabolite of CPT-11, by carboxylesterases. SN-38 exhibits up to 1,000-fold more potent cytotoxic activity against various cancer cells *in vitro* than CPT-11 (10). Although CPT-11 is converted to SN-38 in the liver and tumor, the metabolic conversion rate is <10% of the original volume of CPT-11 (11, 12). In addition, the conversion of CPT-11 to SN-38 depends on the genetic interindividual variability of carboxylesterase activity (13). Thus, direct use of SN-38 might be of great advantage and attractive for cancer treatment. For the clinical use of SN-38, however, it is essential to develop a soluble form of water-insoluble SN-38. The progress of the manufacturing technology of "micellar nanoparticles" may make it possible to use SN-38 for *in vivo* experiments and further clinical use.

Passive targeting of drug delivery system is based on the pathophysiologic characteristics that are observed in many solid tumors: hypervascularity, irregular vascular architecture, potential for secretion of vascular permeability factors, and the absence of effective lymphatic drainage that prevents efficient clearance of macromolecules. These characteristics, unique to solid tumors, are believed to be the basis of the enhanced permeability and retention effect (14–17). Supramolecular structures, such as liposomes and polymeric micelles, are expected to increase the accumulation of drugs in tumor tissue through these pathophysiologic features. Polymeric micelle–based anticancer drugs have been developed in recent years (18–20), and some of them have been under evaluation for clinical trials (21–23). This carrier system can incorporate various kinds of drugs into the inner core by chemical conjugation or physical entrapment with relatively high stability, and the size can be controlled within the range of 20 to 100 nm in diameter. This range of diameters is too large to pass through normal vessel walls; therefore, the drug can be expected to reduce side effects due to a decrease in volume of distribution.

Angiogenesis is essential for the growth and metastasis of solid tumors (24). The clinical importance of angiogenesis in human tumors was shown by several reports indicating a positive relationship between the blood vessel density in the tumor mass and poor prognosis for survival in patients with various types of cancers (25–28). Furthermore, Natsume et al. (29) reported that the antitumor activities of anticancer agents, including *cis*-diammine-dichloroplatinum, vincristine, and docetaxel, were less active against vascular endothelial growth factor (VEGF)–secreting cells, SBC-3/VEGF, *in vivo* as compared with its mock transfectant (SBC-3/Neo), although the high vascularity should have been favorable for the drug delivery.

VEGF is also well known as a potent vascular permeability factor (30). The ability of supramolecular structures to accumulate in target tissue is based on the enhanced tumor angiogenesis and tumor vascular permeability that occur in solid tumors. Therefore, we hypothesized that a polymeric micelle–based drug carrier would increase its accumulation and deliver enhanced therapeutic efficacy in tumors that secrete higher levels of VEGF. In the present study, we present the superiority of NK012 over CPT-11 in a tumor model,

Requests for reprints: Yasuhiro Matsumura, Investigative Treatment Division, Research Center for Innovative Oncology, National Cancer Center Hospital East, 6-5-1 Kashiwanoha, Kashiwa, Chiba 277-8577, Japan. Phone: 81-4-7134-6857; Fax: 81-4-7134-6857; E-mail: yhmatsum@east.ncc.go.jp.

doi:10.1158/0008-5472.CAN-06-1605

especially in a VEGF-secreting tumor, and we illustrate the outstanding advantage of polymeric micelle–based drug carriers.

Materials and Methods

Drugs and Cells

SN-38 was synthesized by Nippon Kayaku Co., Ltd. (Tokyo, Japan). CPT-11 was purchased from Yakult Honsha Co., Ltd. (Tokyo, Japan). Human colon cancer cell lines WiDR, SW480, Lovo, and HT-29 and human non–small-cell lung cancer cell line A431 were purchased from American Type Culture Collection (Rockville, MD). Human small-cell lung cancer cell line SBC-3 and human non–small-cell lung cancer cell line PC-14 were kindly provided by Dr. I. Kimura (Okayama University, Okayama, Japan) and Dr. Y. Hayata (Tokyo Medical University, Tokyo, Japan), respectively. SBC-3 and PC-14 were maintained in RPMI 1640 supplemented with 10% fetal bovine serum (Cell Culture Technologies, Gaggenau-Hoerden, Germany), penicillin, streptomycin, and amphotericin B (100 units/mL, 100 μg/mL, and 25 μg/mL, respectively; Sigma, St. Louis, MO) in a humidified atmosphere of 5% CO_2 at 37°C. Other cell lines were maintained in DMEM (Nikken Bio Med. Lab., Kyoto, Japan) supplemented with 10% fetal bovine serum. SBC-3/Neo and SBC-3/VEGF were generated from SBC-3 cells that were transfected with BMG-Neo and BMG-Neo-VEGF as previously reported (29). The full-length sequence of human VEGF expressing 206 amino acids (31) was selected. SBC-3/VEGF cells express ~100 times more soluble VEGF than SBC-3/Neo and SBC-3 cells in the supernatant of cultured cells as shown by ELISA (29).

Preparation of an SN-38–Conjugated Poly(Ethylene Glycol)-Poly(Glutamic Acid) Block Copolymer for NK012 Construction

Poly(ethylene glycol)-poly(glutamic acid) block copolymer [PEG-PGlu(SN-38)] was synthesized as follows: A poly(ethylene glycol)-poly(glutamic acid) block copolymer [PEG-PGlu] was prepared according to the previously reported technique (32, 33). SN-38 was covalently introduced into the PGlu segment by the condensation reaction between the carboxylic acid on PGlu and the phenol on SN-38 with 1,3-diisopropylcarbodiimide and *N,N*-dimethylaminopyridine at 26°C. Consequently, the PGlu segment obtained sufficient hydrophobicity. Accordingly, NK012 was constructed with self-assembling PEG-PGlu(SN-38) amphiphilic block copolymers in an aqueous milieu.

Determination of the Size Distribution of NK012 and Drug Release Behavior of SN-38 from NK012

The size distribution of NK012 was measured with the dynamic light scattering method at 25°C using a Particle Sizer NICOMP 380ZLS (Particle Sizing Systems, Santa Barbara, CA). The release behavior of SN-38 from NK012 was investigated *in vitro* at 20°C or 37°C in PBS (pH 7.3) or 5% glucose solution (pH 4.6). The concentration was 0.1 mg/mL. The amount of SN-38 released from NK012 was estimated by UV measurement at 265 nm.

In vitro Growth Inhibition Assay

The growth inhibitory effects of NK012, SN-38, and CPT-11 were examined with a 3-(4,5-dimethylthiazol-2-yl)-2,5-diphenyltetrazolium bromide (MTT) assay. One hundred eighty microliters of an exponentially growing cell suspension (6×10^3/mL-12×10^3/mL) were seeded into a 96-well microtiter plate, and 20 μL of various concentrations of each drug were added. After incubation for 72 hours at 37°C, 20 μL of MTT solution (5 mg/mL in PBS) were added to each well and the plates were incubated for an additional 4 hours at 37°C. After centrifuging the plates at 200 × *g* for 5 minutes, the medium was aspirated from each well, and 180 μL of DMSO were added to each well to dissolve the formazan. The growth inhibitory effect of each drug was assessed spectrophotometrically (SpectraMax 190, Molecular Devices Corp., Sunnyvale, CA).

In vivo Growth Inhibition Assay

The animal experimental protocols were approved by the Committee for Ethics of Animal Experimentation and the experiments were conducted in accordance with the Guidelines for Animal Experiments in the National Cancer Center or Nippon Kayaku.

Experiment 1. Female BALB/c nude mice, 7 weeks old, were purchased from CLEA Japan (Tokyo, Japan). Human colorectal cancer HT-29 cells were grown as s.c. tumor in the flank of the mice. The tumors were excised from the mice and fragments were inoculated s.c. in the mouse flank. When the tumor volume reached 70 to 170 mm^3, mice were randomly divided into test groups consisting of six mice per group (day 0). Drugs were administered on days 0, 4, and 8 by i.v. injection into the tail vein. NK012 was given at doses of 30 (maximum tolerated dose), 15, and 7.5 mg/kg/d. The reference drug, CPT-11, was given at the maximum tolerated dose, 66.7 mg/kg/d, in the optimal schedule reported (34). The length (a) and width (b) of the tumor mass were measured twice a week, and the tumor volume (TV) was calculated as follows: $TV = (a \times b^2) / 2$. Relative tumor volumes at day n were calculated according to the following formula: $RTV = TV_n / TV_0$, where TV_n is the tumor volume at day n, and TV_0 is the tumor volume at day 0. Differences in relative tumor sizes between the treatment groups at day 21 were analyzed with an unpaired t test.

Experiment 2. As a hypervascular tumor model, we used SBC-3/VEGF cells. SBC-3/Neo or SBC-3/VEGF cells (10^7) were s.c. injected into the back of mice. NK012 or CPT-11 was administered when the mean tumor volumes ($n = 4$) reached a massive size of 1,500 mm^3, which gave tumors almost 1.5 cm in length. It took ~65 days for SBC-3/Neo and 20 days for SBC-3/VEGF to reach the tumor volume of 1,500 mm^3 from the day of inoculation. NK012 at a dose of 10 or 20 mg/kg/d and CPT-11 at a dose of 15 or 30 mg/kg/d were administered i.v. on days 0, 4, and 8. Differences in tumor sizes between the treatment groups and control group at day 14 were analyzed with an unpaired t test.

Histologic and Immunohistochemical Analysis

Histologic sections were taken from SBC-3/Neo and SBC-3/VEGF tumor tissues when the volumes reached 1,500 mm^3. After extirpation, tissues were fixed with 3.9% formalin in PBS (pH 7.4), and the subsequent preparations and H&E staining were done by Tokyo Histopathologic Laboratory Co., Ltd. (Tokyo, Japan). For detection of tumor blood vessels, polyclonal anti–von Willebrand factor antibody (Dako, Glostrup, Denmark) was used.

Assay for SN-38 and CPT-11 in Plasma and Tissues

Female BALB/c nude mice bearing HT-29 (as mentioned in experiment 1; $n = 3$) were used for the analysis of the biodistribution of NK012 and CPT-11. NK012 (30 mg/kg) or CPT-11 (66.7 mg/kg) was administered i.v. to the mice. Under anesthesia, blood and tumor samples were taken at 5 minutes, 1, 6, 24, 48, 72, and 168 hours after administration of NK012 and at 5 minutes, 1, 3, 6, and 24 hours after administration of CPT-11. The blood samples were collected in microtubes and immediately centrifuged at 1,600 × *g* for 15 minutes. The plasma and tumor samples were stored at −80°C until analysis.

For the biodistribution study in hypervascular tumors (experiment 2), female BALB/c nude mice ($n = 3$) bearing 1,500-mm^3 massive SBC-3/Neo and SBC-3/VEGF tumors were used. NK012 (20 mg/kg) and CPT-11 (30 mg/kg) were administered on day 0. The mice were sacrificed at 1, 6, 24, and 72 hours (day 3) after administration. The tumor, liver, spleen, upper small intestine, lung, and blood were taken and stored at −80°C until analysis.

Preparation of the free SN-38 (polymer-unbound SN-38) and CPT-11. Tumor samples were homogenized on ice using a Digital homogenizer (Iuchi, Osaka, Japan) and suspended in the mixture of 100 mmol/L glycine-HCl buffer (pH 3)/methanol (1:1, v/v) at a concentration of 5% w/w. The concentrations of free SN-38 and CPT-11 in the plasma and tumor from aliquots of the homogenates (100 μL) and plasma (50 μL) were determined by high-performance liquid chromatography. For free SN-38 (polymer-unbound SN-38) and CPT-11, proteins were precipitated with an ice-cold mixture of methanol/H_2O/$HClO_4$ (50:45:5, v/v/v) containing CPT as an internal standard. The sample was vortexed for 10 seconds, filtered through a MultiScreen Solvinert (Millipore Corp., Bedford, MA), and analyzed.

Preparation of the polymer-bound SN-38 (SN-38 remaining bound to PEG-PGlu). To permit complete release of SN-38 from the conjugate, 20 μL of plasma and 100 μL of tissue samples were diluted with 20 μL of methanol (50%, v/v) and 20 μL of NaOH (0.3 mol/L for plasma and 0.7 mol/L for tissue). The samples were incubated for 15 minutes at 25°C. After incubation, 20 μL of HCl (0.3 mol/L for plasma and 0.7 mol/L for tissue) and 60 μL of internal standard solution were added to the samples, and then the hydrolysis was filtered through a MultiScreen Solvinert. The filtrate was applied to the high-performance liquid chromatography system.

High-performance liquid chromatography. Reversed-phase high-performance liquid chromatography was done at 35°C on a Mightysil RP-18 GP column 150 × 4.6 mm (Kanto Chemical Co., Inc., Tokyo, Japan). The samples were injected into an Alliance Waters 2795 high-performance liquid chromatography system (Waters, Milford, MA) equipped with a Waters 2475 multi λ fluorescence detector. The detector was set at 365 and 430 nm (excitation and emission, respectively) for CPT-11 and CPT, and at 365 and 540 nm for SN-38. A reversed-phase column was used at 35°C. The mobile phase was a mixture of 100 mmol/L ammonium acetate (pH 4.2) and methanol [11:9 (v/v) for SN-38 in plasma and tumor, 3:2 (v/v) for CPT-11 in plasma, and 63:37 (v/v) for CPT-11 in tumor]. The flow rate was 1.0 mL/min. Peak data were recorded with a chromatography management system (Empower, Waters). Polymer-bound SN-38 was determined by subtraction of polymer-unbound SN-38 from the total SN-38 of the hydrolysate.

Pharmacokinetic and Statistical Analyses

The concentrations of SN-38 and CPT-11 in plasma and tissue were fitted to a pharmacokinetic model by the nonlinear least-square method using WinNonlin Professional software (version 4.1; Pharsight Corp., Palo Alto, CA). We used a noncompartmental analysis. The pharmacokinetic variables were calculated using the following equations (AUC_{last} was calculated by the trapezoidal rule to the last measurable data point):

$$AUC_{inf.} = \int_0^{\infty} C(t)dt$$

$$T_{1/2z}(\text{terminal half} - \text{life}) = 0.693/\lambda z$$

(λz is first-order rate constant associated with the terminal portion of the curve)

$$CL_{tot} = \text{Dose}/AUC_{inf.}$$

$$V_{ss} = MRT \times CL_{tot}(MRT, \text{mean residence time})$$

Data were expressed as mean ± SD. Data were analyzed with the Student's t test when the groups showed equal variances (F test) or with Welch's test when they showed unequal variances (F test). $P < 0.05$ was regarded as statistically significant. All statistical tests were two sided.

Results

Preparation and characterization of NK012. NK012 is an SN-38-loaded polymeric micelle constructed in an aqueous milieu by the self-assembly of an amphiphilic block copolymers, PEG-PGlu(SN-38). The molecular weight of PEG-PGlu(SN-38) was determined to be ~19,000 (PEG segment, 12,000; SN-38-conjugated PGlu segment, 7,000). NK012 was obtained as a freeze-dried formulation and contained ca. 20% (w/w) of SN-38 (Fig. 1*A*). The mean particle size of NK012 is 20 nm in diameter with a relatively narrow range (Fig. 1*B*). The releasing rates of SN-38 from NK012 in PBS at 37°C were 57% and 74% at 24 and 48 hours, respectively, and those in 5% glucose solution at 37°C were 1% and 3% at 24 and 48 hours, respectively (Fig. 1*C*). SN-38 is loaded by chemical bonding to the block copolymer. The bonding is phenyl ester bond, which is stable under acidic condition and labile under mild alkaline condition. These results indicate that NK012 can release SN-38 under neutral condition even without the presence of a hydrolytic enzyme and is stable in 5% glucose solution. It is suggested that NK012 is stable before administration and starts to release SN-38, the active component, under physiologic conditions after administration.

Cellular sensitivity of non–small-cell lung cancer and colon cancer cells to SN-38, NK012, and CPT-11. The IC_{50} values of NK012 for the cell lines ranged from 0.009 μmol/L (SBC-3 cells) to 0.16 μmol/L (WiDR cells). The growth inhibitory effects of NK012 are 43- to 340-fold more potent than those of CPT-11, whereas the IC_{50} values of NK012 were 2.3- to 5.8-fold higher than those of SN-38. NK012 exhibited a higher cytotoxic effect against each cell line as compared with CPT-11 (43- to 340-fold sensitivity). On the other hand, the IC_{50} values of NK012 were a little higher than those of SN-38, similar to the cytotoxic feature also reported in a previous study about micellar drugs (ref. 23; Table 1).

Antitumor activity and pharmacokinetic analysis of NK012 and CPT-11 using HT-29–bearing nude mice (experiment 1). Potent activity was observed in mice treated with NK012 at doses of 15 and 30 mg/kg (Fig. 2*A*), although neither CPT-11 at a dose of 66.7 mg/kg/d nor NK012 at a dose of 7.5 mg/kg/d exerted any significant antitumor activity *in vivo*. Comparison of the relative tumor volume at day 21 revealed significant differences between 15 mg/kg/d NK012 and 66.7 mg/kg/d CPT-11 and between 30 mg/kg/d NK012 and 66.7 mg/kg/d CPT-11 ($P < 0.05$). Although treatment-related body weight loss was observed in mice treated with each drug, body weight recovered by day 21 (Fig. 2*B*). These results clearly show the significant *in vivo* activity of NK012 against HT-29.

After injection of CPT-11, the concentrations of CPT-11 and SN-38 for plasma declined rapidly with time in a log-linear fashion. On the other hand, NK012 (polymer-bound SN-38) exhibited slower clearance (Fig. 3*A*). The clearance of NK012 in the HT-29 tumor was significantly slower and the concentration of free SN-38 was maintained at >30 ng/g even at 168 hours after injection (Fig. 3*B*). The pharmacokinetic variables of each drug in the plasma and tumor are depicted in Table 2.

Tumor-to-plasma concentration ratios (Kp) of polymer-bound and free SN-38 increased during the observation period. The highest value of Kp was achieved at 168 hours after administration, 108 for polymer-bound and 11.0 for free SN-38 (Table 3). These results indicate that NK012 can remain in the tumor tissue for a longer period and release free SN-38.

Antitumor activity and the distribution of NK012 and CPT-11 in SBC-3/Neo or SBC-3/VEGF tumors (experiment 2). To determine whether the potent antitumor effect of NK012 is enhanced in the tumors with high vascularity, we used VEGF-secreting cells SBC-3/VEGF. There was no significant difference in the *in vitro* cytotoxic activity of each drug between SBC-3/Neo and SBC-3/VEGF (Fig. 4*A*). SBC-3/VEGF tumors are reddish by gross evaluation as compared with SBC-3/Neo tumors (Fig. 4*B*). Histologic and immunohistochemical (von Willebrand factor) examination revealed that prominent leakage of erythrocytes and high vascularity were observed in SBC-3/VEGF tumor xenografts. On the other hand, SBC-3/Neo tumors have less tumor vasculatures and more interstitial space as compared with SBC-3/VEGF tumors

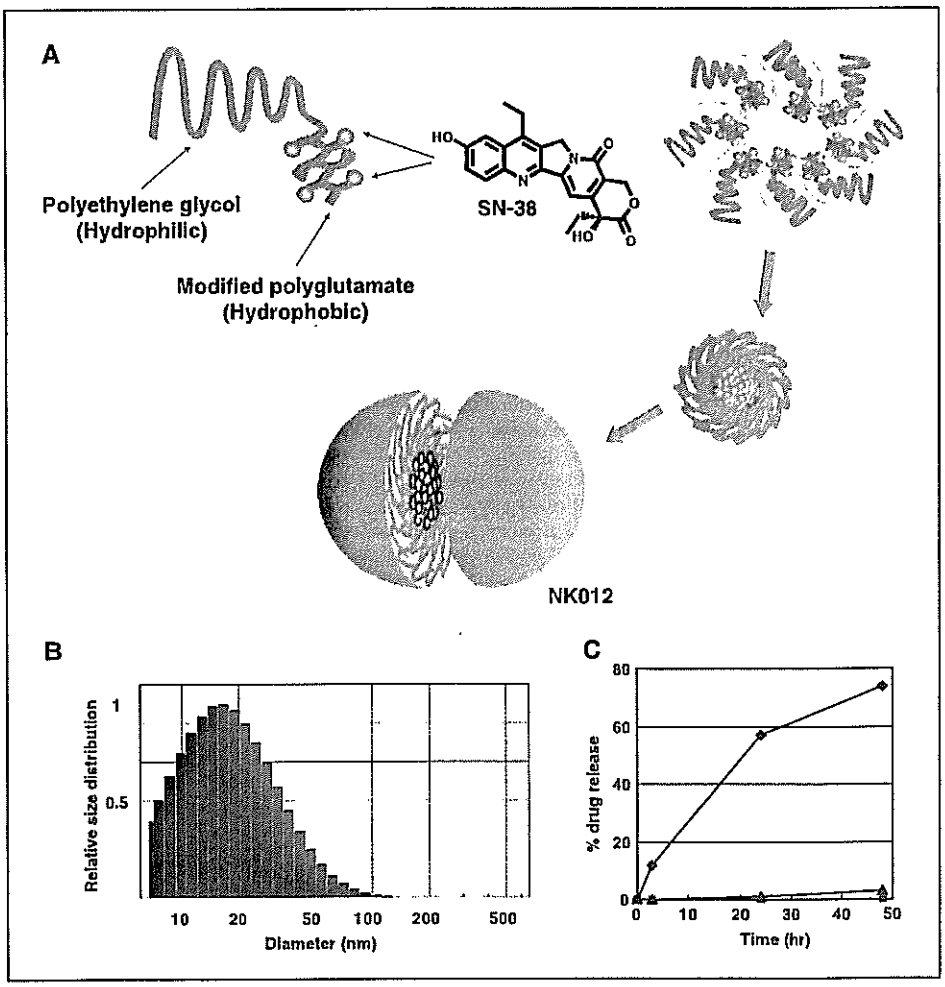

Figure 1. Preparation and characterization of NK012. *A*, schematic structure of NK012. A polymeric micelle carrier of NK012 consists of a block copolymer of PEG (molecular weight of ~12,000) and partially modified polyglutamate (~20 units). PEG (hydrophilic) is believed to be the outer shell and SN-38 was incorporated into the inner core of the micelle. *B*, size distribution of NK012 measured with the dynamic light scattering method. The *Y* axis shows relative particle size distribution. *C*, release of free SN-38 from the micelles in PBS [pH 7.3, 37°C (♦)] or 5% glucose solution [pH 4.6, 20°C (■), 37°C (▲)].

(Fig. 4*B*). Deviating from the ordinary experimental tumor model, tumors were allowed to grow until they became massive in size, ~1.5 cm (Fig. 4*C*), and then the treatment was initiated. NK012 at doses of 15 and 30 mg/kg showed potent antitumor activity against bulky SBC-3/Neo tumors (1,533.1 ± 1,204.7 mm^3) as compared with CPT-11 (Fig. 4*C*). Striking antitumor activity was observed in mice treated with NK012 (Fig. 4*C*) when we compared the antitumor activity of NK012 with that of CPT-11 using SBC-3/VEGF cells. SBC-3/VEGF bulky masses (1,620.7 ± 834.0 mm^3) disappeared in all mice, although relapse 3 months after treatment was noted in one mouse treated with NK012 20 mg/kg. On the other hand, SBC-3/VEGF were not eradicated and rapidly regrew after a partial response in mice treated with CPT-11. Approximately 10% body weight loss was observed in mice treated with 20 mg/kg NK012, but no significant difference was observed in comparison with mice treated with 30 mg/kg CPT-11.

We then examined the distribution of free SN-38 in the SBC-3/Neo and SBC-3/VEGF masses after administration of NK012 and CPT-11. In the case of CPT-11 administration, the concentrations at 1 and 6 hours after the administration were <100 ng/g both in the SBC-3/Neo and SBC-3/VEGF tumors and were almost negligible at 24 hours in both tumors (Fig. 5*A*). There was no significant difference in the concentration between the SBC-3/Neo and SBC-3/VEGF tumors. On the other hand, in the case of NK012 administration, free SN-38 was detectable in the tumors even at 72 hours after the administration. The concentrations of free SN-38 were higher in the SBC-3/VEGF tumors than those in the SBC-3/Neo tumors at any time point during the period of observation (significant at 1, 6, and 24 hours; $P < 0.05$; Fig. 5*A*).

Tissue distribution of SN-38 after administration of NK012 and CPT-11. We examined the concentration-time profile of free SN-38 in various tissues after i.v. administration of NK012 and

Table 1. *In vitro* growth inhibitory activity of SN-38, NK012, and CPT-11 in human lung and colorectal cancer cells (MTT assay)

Cell line	IC_{50} (μmol/L)		
	SN-38	NK012	CPT-11
WiDR	0.046 ± 0.008	0.16 ± 0.014	20.4 ± 1.6
SW480	0.025 ± 0.003	0.11 ± 0.028	31.9 ± 1.3
Lovo	0.0067 ± 0.0012	0.026 ± 0.003	7.24 ± 1.04
HT-29	0.016 ± 0.003	0.068 ± 0.007	23.1 ± 2.63
PC-14	0.044 ± 0.025	0.14 ± 0.021	5.96 ± 0.90
SBC-3	0.0016 ± 0.001	0.0093 ± 0.005	0.72 ± 0.22
A431	0.0081 ± 0.002	0.019 ± 0.007	5.6 ± 1.5

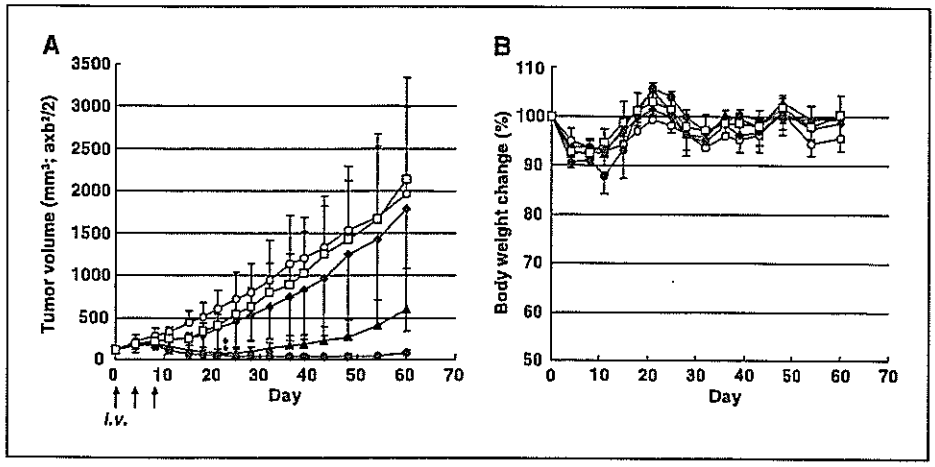

Figure 2. The effect of NK012 and CPT-11 against an HT-29 tumor xenograft. *A*, HT-29 tumor was inoculated s.c. into the flank of mice as described in Materials and Methods. CPT-11 at a dose of 66.7 mg/kg/d (□), NK012 at a dose of 7.5 mg/kg/d (♦), NK012 at a dose of 15 mg/kg/d (▲), or NK012 at a dose of 30 mg/kg/d (●) was administered i.v. on days 0, 4, and 8 (○, no treatment). Tumor volume in mice treated with CPT-11 or NK012. *Points*, mean; *bars*, SD. *, $P < 0.05$. *B*, treatment-related body weight loss occurred in mice treated with CPT-11 and NK012. *Points*, mean; *bars*, SD.

CPT-11. All organs measured exhibited the highest concentration of SN-38 at 1 hour after administration in mice given CPT-11 (Fig. 5*B*). On the other hand, mice given NK012 exhibited prolonged distribution in the liver and spleen (Fig. 5*B*). In a similar manner to other micellar drugs (19, 23), NK012 showed relatively higher accumulation in organs of the reticuloendothelial system. In the lung, kidney, and small intestine, the highest concentration of free SN-38 was achieved at 1 hour after injection of NK012 and the concentration was almost negligible at 24 hours. Although relatively high at 1 hour after administration of NK012 and CPT-11, the concentrations of free SN-38 in the small intestine rapidly decreased. Interestingly, there was no significant difference in the kinetic character of free SN-38 in the small intestine between mice treated with NK012 and CPT-11.

Discussion

The drug-incorporating polymeric micelle has characteristic pharmacokinetic features. These structures are too large to pass through normal vessel walls and evade renal excretion. The outer shell of the drug with PEG diminishes nonspecific capture by the reticuloendothelial system. Therefore, the drug can be expected to achieve a long half-life, which permits a large amount of the drug-incorporating micelles to reach the tumor site through the enhanced permeability and retention effect. The pharmacokinetic study revealed that the plasma AUC of polymer-bound SN-38 after administration of NK012 at a dose of 30 mg/kg to the HT-29-bearing mice was ~200-fold higher than that of CPT-11 at a dose of 66.7 mg/kg. A 14-fold higher AUC of the free SN-38 was achieved in mice given NK012 compared with mice given CPT-11. Prolonged circulation of NK012 in the blood might increase the accumulation of NK012 in a tumor tissue due to the enhanced permeability and retention effect. In fact, the tumor concentration of free SN-38 at 24 hours after administration of NK012 reached 90.4 ng/g and high concentrations were maintained up to 168 hours (53.1 ng/g for 48 hours, 42.6 ng/g for 72 hours, and 35.8 ng/g for 168 hours). This range of concentrations can exert sufficient antitumor activity against tumor cells. On the other hand, the concentration of CPT-11 was only 4.5 ng/g at 24 hours. These results indicate that the enhancement of tumor distribution closely contributes to the potent antitumor activity of NK012 *in vivo*.

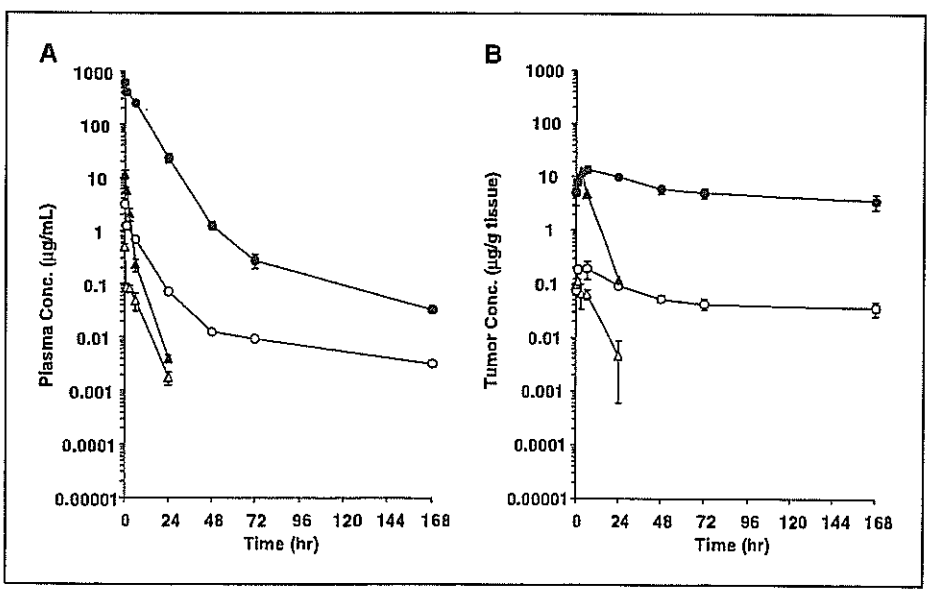

Figure 3. Plasma and tumor concentrations of respective analytes after an i.v. administration of CPT-11 (66.7 mg/kg) or NK012 (30 mg/kg) to HT-29-bearing nude mice. *A*, plasma. *B*, tumor. ●, polymer-bound SN-38; ○, free SN-38 (polymer-unbound SN-38); △, SN-38 converted from CPT-11; ▲, CPT-11.

Table 2. Pharmacokinetic variables of analytes in plasma and tumor after an i.v. administration of NK012 or CPT-11 to nude mice bearing human colon cancer HT-29 cells (NK012, 30 mg/kg; CPT-11, 66.7 mg/kg)

	Test article		C_{max} (μg/mL)	T_{max} (h)	$T_{1/2z}$ (h)	AUC_{last} (μg h/mL)	AUC_{inf} (μg h/mL)	CL_{tot} (mL/h/kg)	V_{ss} (mL/kg)	MRT_{last} (h)	$MRT_{inf.}$ (h)
Plasma	NK012	P-b SN-38*	—†	—	31.4	5,000	5,010	5.99	40.4	6.68	6.74
		P-u SN-38‡	3.10	0.0833	61.7	15.5	15.8	—	—	10.8	15.3
	CPT-11	CPT-11	—	—	3.08	22.1	22.2	3,010	5,420	1.78	1.80
		SN-38	0.488	0.0833	3.76	1.10	1.11	—	—	3.82	4.04
Tumor	NK012	P-b SN-38	13.8	6	—	1,010	—	—	—	62.8	—
		P-u SN-38	0.188	6	—	10.2	—	—	—	58.1	—
	CPT-11	CPT-11	12.6	3	3.36	99.7	100	—	—	4.41	4.55
		SN-38	0.108	1	4.75	1.07	1.10	—	—	5.20	5.92

NOTE: Three female nude mice were used for the analysis of biodistribution of SN-38 and CPT-11 in plasma and tissues. Data were expressed as means.
*Polymer-bound SN-38; SN-38 remaining bound to PEG-PGlu.
†Not determined.
‡Polymer-unbound SN-38; free SN-38 from PEG-PGlu.

Several preclinical studies on cytotoxic agent–incorporating polymeric micelles show their advantage as anticancer agents *in vivo* as compared with drugs of small molecular size (19, 22, 23). Because the advantage of passive targeting has been explained by the enhanced permeability and retention theory, it is essential to elucidate the correlation between the effectiveness of micellar drugs and tumor hypervascularity and hyperpermeability. We hypothesized that a polymeric micelle–based drug carrier could increase its accumulation in the tumor site and could thus enhance the therapeutic efficacy in tumors with high vascularity. To ascertain the hypothesis, we used SBC-3/VEGF. We adopted a bulky tumor model for our *in vivo* experiment to clarify the difference in activity against SBC-3/Neo and SBC-3/VEGF tumors. Histologic examination of SBC-3/VEGF showed hypervascularity and prominent leakage of erythrocytes. On the other hand, SBC-3/Neo showed hypovascularity. Our *in vivo* experiment showed that NK012 obviously enhanced its antitumor activity in SBC-3/VEGF-inplanted mice and eradicated bulky masses. It was thought that the sensitivity of cells to NK012 might not change *in vivo* because the *in vitro* sensitivity of NK012 was almost equivalent between SBC-3/Neo and SBC-3/VEGF cells. When we compared the distribution of NK012 (free SN-38) in the tumor sites, significantly enhanced accumulation was observed in the SBC-3/VEGF tumors. This strongly suggested that the drug distribution throughout the tumor site was enhanced by the hypervascularity and hyperpermeability induced by VEGF, and, subsequently, higher antitumor activity was achieved. High vascular density and enhanced vascular permeability might also be favorable for drug delivery of low molecular weight drugs. However, the SN-38 concentration was not significantly high in SBC-3/VEGF tumors after the administration of CPT-11, and tumors exhibited rapid regrowth after the treatment. We assume that such conventional low molecular size anticancer agents almost disappear from the bloodstream without being subjected to the enhanced permeability and retention effect before they can reach the target organs (solid tumor). The fact of correlation between the blood vessel density in

Table 3. Tumor-to-plasma concentration ratio (Kp) of analytes after an i.v. administration of NK012 (30 mg/kg) to nude mice bearing human colon cancer HT-29 cells

Test article	Analyte		Time after administration (h)						
			0.0833	1	6	24	48	72	168
NK012	P-b SN-38*	Plasma (μg/mL)	612	410	254	23.3	1.25	0.278	0.0333
		Tumor (μg/g)	4.99	8.00	13.8	9.95	5.90	5.03	3.58
		Kp† (mL/g)	0.00815	0.0195	0.0543	0.427	4.72	18.1	108
	P-u SN-38‡	Plasma (μg/mL)	3.10	1.24	0.673	0.0717	0.0127	0.00925	0.00325
		Tumor (μg/g)	0.0763	0.187	0.188	0.0904	0.0531	0.0426	0.0358
		Kp (mL/g)	0.0246	0.151	0.279	1.26	4.18	4.61	11.0

NOTE: Data were expressed as means of three mice.
*Polymer-bound SN-38; SN-38 remaining bound to PEG-PGlu.
†Kp values were calculated on the mean concentrations of three mice.
‡Polymer-unbound SN-38; free SN-38 from PEG-PGlu.

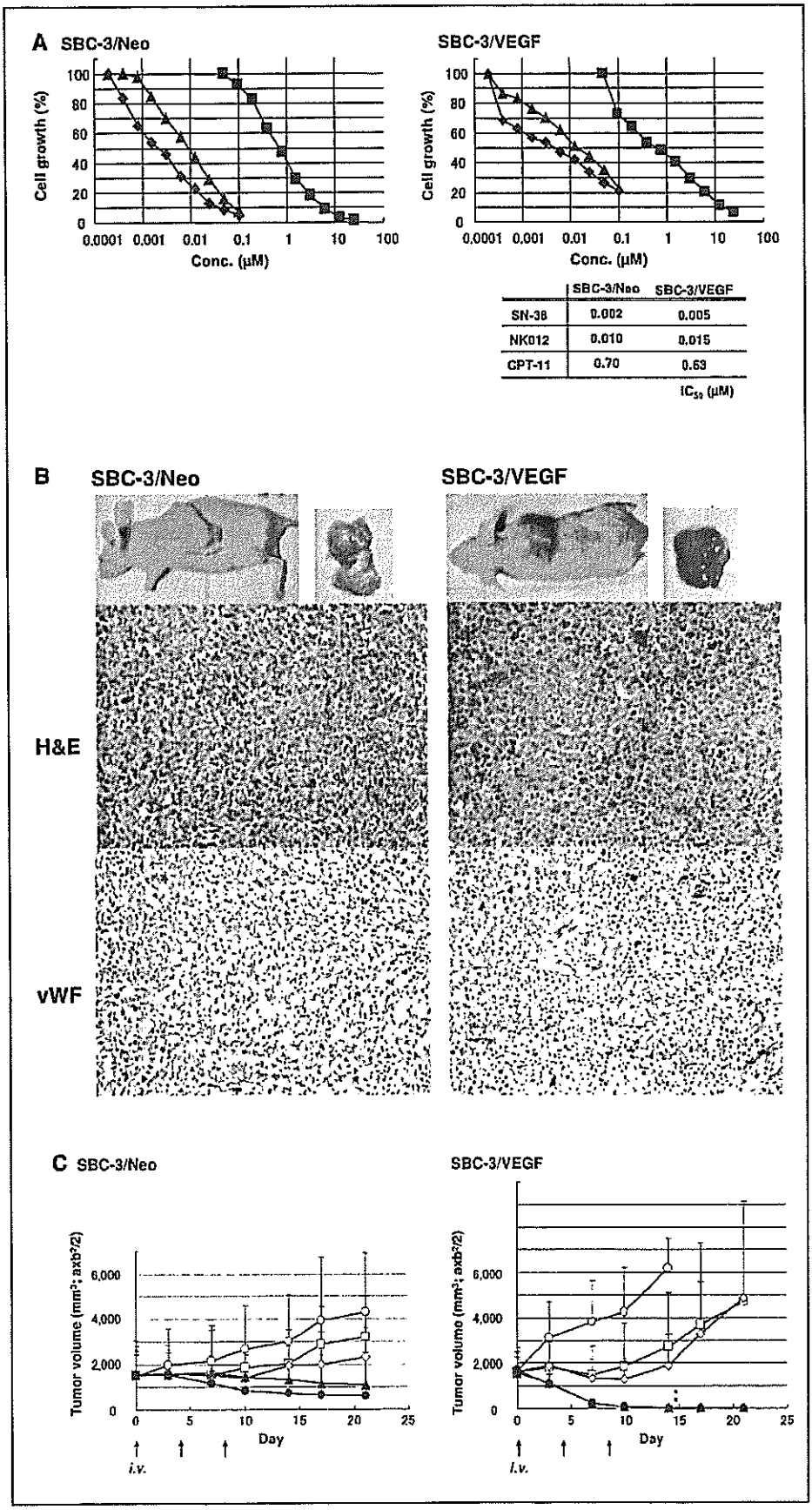

	SBC-3/Neo	SBC-3/VEGF
SN-38	0.002	0.005
NK012	0.010	0.015
CPT-11	0.70	0.63

IC_{50} (μM)

Figure 4. Growth inhibitory effect of NK012, SN-38, and CPT-11 on SBC-3/Neo and SBC-3/VEGF cells. *A*, in *in vitro* experiment, the cells were exposed to the indicated concentrations of each drug for 72 hours. The growth inhibition curves and IC_{50} values for NK012 (▲), SN-38 (◆), and CPT-11 (■) are shown. *B*, representative photographs of massive tumors developed from SBC-3/Neo and SBC-3/VEGF at the time just before treatment initiation. Histologic (H&E, ×20) and immunohistochemical (von Willebrand factor, ×20) examinations for each tumor are shown. *C*, i.v. administration of NK012 or CPT-11 was started when the mean tumor volumes of groups reached a massive size of 1,500 mm³. The mice were divided into test groups (○, control; □, CPT-11 15 mg/kg/d; ◇, CPT-11 30 mg/kg/d; ▲, NK012 10 mg/kg/d; ●, NK012 20 mg/kg/d). NK012 or CPT-11 was administered i.v. on days 0, 4, and 8. Each group consisted of four mice. *, $P < 0.05$.

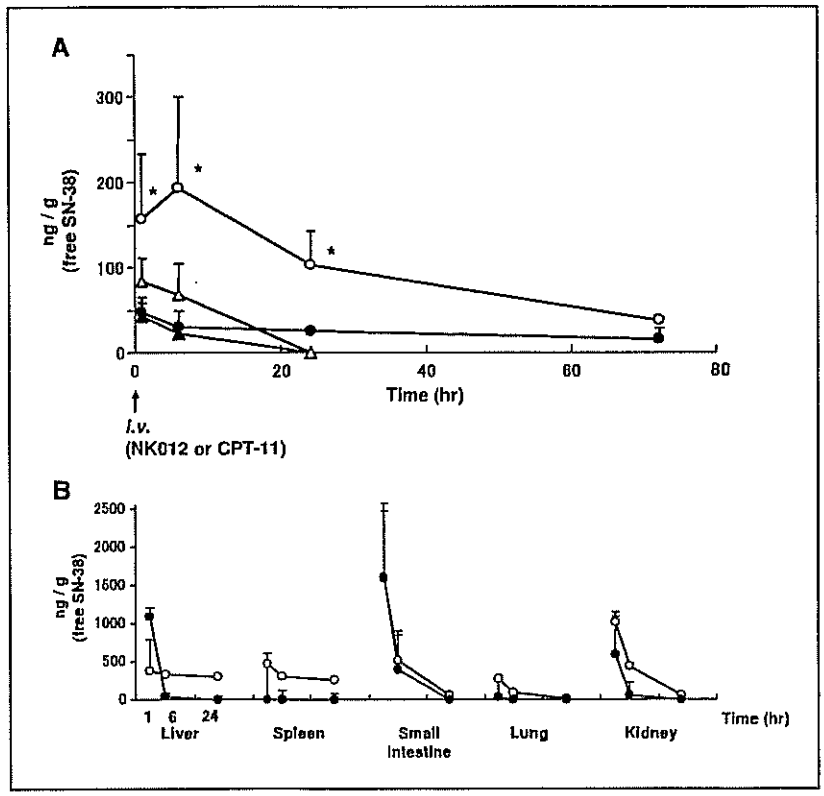

Figure 5. Tissue and tumor distribution of free SN-38 after administration of NK012 and CPT-11. *A*, time profile of free SN-38 concentration in SBC-3/Neo (●, NK012 20 mg/kg/d; ▲, CPT-11 30 mg/kg/d) and SBC-3/VEGF (○,NK012 20 mg/kg/d; △, CPT-11 30 mg/kg/d). NK012 on days 0 and 4 (96 hours) or CPT-11 on day 0 was administered. *, $P < 0.05$. *B*, tissue distribution of free SN-38 after single injection of NK012 at 30 mg/kg (○) and CPT-11 at 40 mg/kg (●).

the tumor mass and poor prognosis for survival in people with various types of cancers (25–28) supports the idea that low molecular weight drugs are not so effective in the treatment of solid tumors, which are rich in blood vessels.

Jain (35) reported that the convective passage of large drug molecules into the core of solid tumors could be impeded by abnormally high interstitial pressures in solid tumors. However, he also considered that low molecular weight anticancer agents might be harmful to normal organs because they can leak out of normal blood vessels freely; he finally concluded that one useful strategy for evading the barriers to drug dispersion would be to inject patients with drug carriers, such as liposome, filled with low molecular weight drugs. NK012 has the potential to allow the effective sustained release of SN-38 inside a tumor following the accumulation of NK012 into tumor tissue. As a matter of fact, substantial amount of SN-38 is expected to be released from the polymeric micelle. Consequently, released SN-38 becomes distributed throughout the tumor tissue and internalizes into cancer cells to kill them.

In recent years, the novel liposome-based formulation of SN-38 (LE-SN38) has been developed (36). LE-SN38 shows promising antitumor activity against various cancer cell lines (37, 38) and a clinical trial to assess its efficacy is now under way (39). The release of SN-38 from LE-SN38 is very slow as compared with NK012, ~1.9% of the drug being released from LE-SN38 in PBS buffer over 120 hours (36). The size of LE-N38 ranges from 150 to 200 nm. On the other hand, the particle size of NK012 is ~20 nm. Interestingly, Unezaki et al. (40) reported that fluorescence-labeled PEG liposomes were densely located outside the tumor vessels and stayed around the vessel walls for 2 days after i.v. injection. These data suggest that the PEG liposome is too large to move freely in the tumor interstitium and too stable to be released easily. The difference in size distribution and the character of the drug release between NK012 and LE-SN38 might influence their clinical effectiveness in the treatment of solid tumors.

One of the major toxicities associated with CPT-11 administration is severe diarrhea. Although the mechanism of the diarrhea has not yet been elucidated, one possible explanation is structural and functional injuries to the gastrointestinal tract owing to the mitotic inhibitory activity of SN-38 and CPT-11. It was reported that the number of episodes of diarrhea had a better correlation with the plasma AUC of SN-38 than with CPT-11 (41). In the present study, no difference in SN-38 accumulations in the small intestine was seen when equimolar NK012 (20 mg/kg) and CPT-11 (30 mg/kg) were administered. We also reported, using a rat mammary tumor model, that NK012 showed significant antitumor effect with diminishing incidence of diarrhea as compared with CPT-11 (42). These results suggest that diarrhea, one of the dose-limiting toxicities of CPT-11, is not augmented by the administration of NK012.

In conclusion, the present data suggest that NK012 possesses a treatment advantage over CPT-11, especially in hypervascular tumors such as renal cell carcinomas, medulloblastomas, and hepatocellular carcinomas. We have now started a phase I clinical trial for NK012 in patients with advanced solid tumors.

Acknowledgments

Received 5/3/2006; revised 7/20/2006; accepted 8/21/2006.

The costs of publication of this article were defrayed in part by the payment of page charges. This article must therefore be hereby marked *advertisement* in accordance with 18 U.S.C. Section 1734 solely to indicate this fact.

References

1. Li LH, Fraser TJ, Olin EJ, Bhuyan BK. Action of camptothecin on mammalian cells in culture. Cancer Res 1972;32:2643–50.
2. Gallo RC, Whang-Peng J, Adamson RH. Studies on the antitumor activity, mechanism of action, and cell cycle effects of camptothecin. Natl Cancer Inst 1971; 46:789–95.
3. Gottlieb JA, Guarino AM, Call JB, Oliverio VT, Block JB. Preliminary pharmacologic and clinical evaluation of camptothecin sodium (NSC-100880). Cancer Chemother Rep 1970;54:461–70.
4. Muggia FM, Creaven PJ, Hansen HH, Cohen MH, Selawry OS. Phase I clinical trial of weekly and daily treatment with camptothecin (NSC-100880): correlation with preclinical studies. Cancer Chemother Rep 1972;56: 515–21.
5. Cunningham D, Pyrhonen S, James RD, et al. Randomised trial of irinotecan plus supportive care versus supportive care alone after fluorouracil failure for patients with metastatic colorectal cancer. Lancet 1998; 352:1413–8.
6. Saltz LB, Cox JV, Blanke C, et al. Irinotecan plus fluorouracil and leucovorin for metastatic colorectal cancer. Irinotecan Study Group. N Engl J Med 2000;343: 905–14.
7. Noda K, Nishiwaki Y, Kawahara M, et al. Irinotecan plus cisplatin compared with etoposide plus cisplatin for extensive small-cell lung cancer. N Engl J Med 2002; 346:85–91.
8. Negoro S, Masuda N, Takada Y, et al. CPT-11 Lung Cancer Study Group West. Randomised phase III trial of irinotecan combined with cisplatin for advanced non-small-cell lung cancer. Br J Cancer 2003; 88:335–41.
9. Bodurka DC, Levenback C, Wolf JK, et al. Phase II trial of irinotecan in patients with metastatic epithelial ovarian cancer or peritoneal cancer. J Clin Oncol 2003; 21:291–7.
10. Takimoto CH, Arbuck SG. Topoisomerase I targeting agents: the camptothecins. In: Chabner BA, Lango DL, editors. Cancer chemotherapy and biotherapy: principal and practice. 3rd ed. Philadelphia (PA): Lippincott Williams & Wilkins; 2001. p. 579–646.
11. Slatter JG, Schaaf LJ, Sams JP, et al. Pharmacokinetics, metabolism, and excretion of irinotecan (CPT-11) following I.V. infusion of [(14)C]CPT-11 in cancer patients. Drug Metab Dispos 2000;28:423–33.
12. Rothenberg ML, Kuhn JG, Burris HA III, et al. Phase I and pharmacokinetic trial of weekly CPT-11. J Clin Oncol 1993;11:2194–204.
13. Guichard S, Terret C, Hennebelle I, et al. CPT-11 converting carboxylesterase and topoisomerase activities in tumour and normal colon and liver tissues. Br J Cancer 1999;80:364–70.
14. Matsumura Y, Maeda H. A new concept for macromolecular therapeutics in cancer chemotherapy: mechanism of tumoritropic accumulation of proteins and the antitumor agent smancs. Cancer Res 1986;46: 6387–92.
15. Dvorak HF, Nagy JA, Dvorak JT, Dvorak AM. Identification and characterization of the blood vessels of solid tumors that are leaky to circulating macromolecules. Am J Pathol 1988;133:95–109.
16. Maeda H, Matsumura Y. Tumoritropic and lymphotropic principles of macromolecular drugs. Crit Rev Ther Drug Carrier Syst 1989;6:193–210.
17. Matsumura Y, Maruo K, Kimura M, Yamamoto T, Konno T, Maeda H. Kinin-generating cascade in advanced cancer patients and *in vitro* study. Jpn J Cancer Res 1991;82:732–41.
18. Yokoyama M, Miyauchi M, Yamada N, et al. Characterization and anticancer activity of the micelle-forming polymeric anticancer drug Adriamycin-conjugated poly(ethylene glycol)-poly(aspartic acid) block copolymer. Cancer Res 1990;50:1693–700.
19. Yokoyama M, Okano T, Sakurai Y, Ekimoto H, Shibazaki C, Kataoka K. Toxicity and antitumor activity against solid tumors of micelle-forming polymeric anticancer drug and its extremely long circulation in blood. Cancer Res 1991;51:3229–36.
20. Kataoka K, Harada A, Nagasaki Y. Block copolymer micelles for drug delivery: design, characterization and biological significance. Adv Drug Deliv Rev 2001;47: 113–31.
21. Matsumura Y, Hamaguchi T, Ura T, et al. Phase I clinical trial and pharmacokinetic evaluation of NK911, a micelle-encapsulated doxorubicin. Br J Cancer 2004;91: 1775–81.
22. Hamaguchi T, Matsumura Y, Suzuki M, et al. NK105, a paclitaxel-incorporating micellar nanoparticle formulation, can extend *in vivo* antitumour activity and reduce the neurotoxicity of paclitaxel. Br J Cancer 2005; 92:1240–6.
23. Uchino H, Matsumura Y, Negishi T, et al. Cisplatin-incorporating polymeric micelles (NC-6004) can reduce nephrotoxicity and neurotoxicity of cisplatin in rats. Br J Cancer 2005;93:678–87.
24. Folkman J. Anti-angiogenesis: new concept for therapy of solid tumors. Ann Surg 1972;175:409–16.
25. Gasparini G, Harris AL. Clinical importance of the determination of tumor angiogenesis in breast carcinoma: much more than a new prognostic tool. J Clin Oncol 1995;13:765–82.
26. Dickinson AJ, Fox SB, Persad RA, Hollyer J, Sibley GN, Harris AL. Quantification of angiogenesis as an independent predictor of prognosis in invasive bladder carcinomas. Br J Urol 1994;74:762–6.
27. Takahashi Y, Kitadai Y, Bucana CD, Cleary KR, Ellis LM. Expression of vascular endothelial growth factor and its receptor, KDR, correlates with vascularity, metastasis, and proliferation of human colon cancer. Cancer Res 1995;55:3964–8.
28. Williams JK, Carlson GW, Cohen C, Derose PB, Hunter S, Jurkiewicz MJ. Tumor angiogenesis as a prognostic factor in oral cavity tumors. Am J Surg 1994; 168:373–80.
29. Natsume T, Watanabe J, Koh Y, et al. Antitumor activity of TZT-1027 (Soblidotin) against vascular endothelial growth factor-secreting human lung cancer *in vivo*. Cancer Sci 2003;94:826–33.
30. Stacker SA, Caesar C, Baldwin ME, et al. VEGF-D promotes the metastatic spread of tumor cells via the lymphatics. Nat Med 2001;7:186–91.
31. Amoroso A, Del Porto F, Di Monaco C, Manfredini P, Afeltra A. Vascular endothelial growth factor: a key mediator of neoangiogenesis. A review. Eur Rev Med Pharmacol Sci 1997;1:17–25.
32. Cabral H, Nishiyama N, Okazaki S, Koyama H, Kataoka K. Preparation and biological properties of dichloro(1,2-diaminocyclohexane)platinum(II) (DACHPt)-loaded polymeric micelles. J Controlled Res 2005;101: 223–32.
33. Nishiyama N, Yokoyama M, Aoyagi T, Okano T, Sakurai Y, Kataoka K. Preparation and characterization of self-assembled polymer-metal complex micelle from *cis*-dichlorodiammineplatinum(II) and poly(ethylene glycol)-poly(α,β-aspartic acid) block copolymer in an aqueous medium. Langmuir 1999;15:377–83.
34. Kawato Y, Furuta T, Aonuma M, Yasuoka M, Yokokura T, Matsumoto K. Antitumor activity of a camptothecin derivative, CPT-11, against human tumor xenografts in nude mice. Cancer Chemother Pharmacol 1991;28:192–8.
35. Jain RK. Barriers to drug delivery in solid tumors. Sci Am 1994;271:58–65.
36. Zhang JA, Xuan T, Parmar M, et al. Development and characterization of a novel liposome-based formulation of SN-38. Int J Pharm 2004;270:93–107.
37. Lei S, Chien PY, Sheikh S, Zhang A, Ali S, Ahmad I. Enhanced therapeutic efficacy of a novel liposome-based formulation of SN-38 against human tumor models in SCID mice. Anticancer Drugs 2004;15:773–8.
38. Pal A, Khan S, Wang YF, et al. Preclinical safety, pharmacokinetics and antitumor efficacy profile of liposome-entrapped SN-38 formulation. Anticancer Res 2005;25:331–41.
39. Kraut EH, Fishman MN, LoRusso PM, et al. Final result of a phase I study of liposome encapsulated SN-38 (LE-SN38): safety, pharmacogenomics, pharmacokinetics, and tumor response [abstract 2017]. Proc Am Soc Clin Oncol 2005;23:139s.
40. Unezaki S, Maruyama K, Hosoda JI, et al. Direct measurement of the extravasation of polyethyleneglycol-coated liposomes into solid tumor tissue by *in vivo* fluorescence microscopy. Int J Pharmaceut 1996;144: 11–7.
41. Sasaki Y, Yoshida Y, Sudoh K, et al. Pharmacological correlation between total drug concentration and lactones of CPT-11 and SN-38 in patients treated with CPT-11. Jpn J Cancer Res 1995;86:111–6.
42. Onda T, Nakamura I, Seno C, et al. Superior antitumor activity of NK012, 7-ethyl-10-hydroxycamptothecin-incorporating micellar nanoparticle, to irrinotecan [abstract 3062]. Proc Am Assoc Cancer Res 2006;47: 720s.

British Journal of Cancer (2006) 95, 601–606

www.bjcancer.com

NK105, a paclitaxel-incorporating micellar nanoparticle, is a more potent radiosensitising agent compared to free paclitaxel

T Negishi[1], F Koizumi[1], H Uchino[2], J Kuroda[1], T Kawaguchi[3], S Naito[2] and Y Matsumura[*,1]

[1]Investigative Treatment Division, Research Center for Innovative Oncology, National Cancer Center Hospital East, 6-5-1 Kashiwanoha, Kashiwa, Chiba 277-8577, Japan; [2]Department of Urology, Graduate School of Medical Sciences, Kyushu University, 3-1-1 Maidashi, Higashi-ku, Fukuoka, Fukuoka 812-8582, Japan; [3]Department of Anatomy and Histology, Fukushima Medical University School of Medicine, 1-Hikariga-oka, Fukushima, Fukushima 960-1247, Japan

NK105 is a micellar nanoparticle formulation designed to enhance the delivery of paclitaxel (PTX) to solid tumours. It has been reported to exert antitumour activity *in vivo* and to have reduced neurotoxicity as compared to that of free PTX. The purpose of this study was to investigate the radiosensitising effect of NK105 in comparison with that of PTX. Lewis lung carcinoma (LLC)-bearing mice were administered a single intravenous (i.v.) injection of PTX or NK105; 24 h after the drug administration, a proportion of the mice received radiation to the tumour site or lung fields. Then, the antitumour activity and lung toxicity were evaluated. In one subset of mice, the tumours were excised and specimens were prepared for analysis of the cell cycle distribution by flow cytometry. Combined NK105 treatment with radiation yielded significant superior antitumour activity as compared to combined PTX treatment with radiation ($P = 0.0277$). On the other hand, a histopathological study of lung sections revealed no significant difference in histopathological changes between mice treated with PTX and radiation and those treated with NK105 and radiation. Flow-cytometric analysis showed that NK105-treated LLC tumour cells showed more severe arrest at the G2/M phase as compared to PTX-treated tumour cells. The superior radiosensitising activity of NK105 was thus considered to be attributable to the more severe cell cycle arrest at the G2/M phase induced by NK105 as compared to that induced by free PTX. The present study results suggest that further clinical trials are warranted to determine the efficacy and feasibility of combined NK105 therapy with radiation.
British Journal of Cancer (2006) **95,** 601–606. doi:10.1038/sj.bjc.6603311 www.bjcancer.com
Published online 8 August 2006

Keywords: paclitaxel; NK105; radiosensitiser; polymer micelle; drug delivery system

Paclitaxel (PTX) has been demonstrated to be one of the most effective anticancer agents available at present (Carney, 1996; Khayat *et al*, 2000). Besides its antitumour activity, its ability to induce radiosensitisation has been reported both *in vitro* (Tishler *et al*, 1992; Choy *et al*, 1993; Lokeshwar *et al*, 1995; Rodriguez *et al*, 1995) and *in vivo* (Milas *et al*, 1994, 1995; Cividalli *et al*, 1998) this effect has been attributed to its effect of stabilising microtubules and inducing cell cycle arrest at the G2/M phase, the most radiosensitive phase of the cell cycle (Terasima and Tolmach, 1963; Sinclair and Morton, 1966). As several clinical studies have demonstrated the efficacy of PTX-based chemotherapy combined with radiotherapy, the combined modality is considered to be a potentially important treatment option for lung and breast cancer (Choy *et al*, 1998a, b, 2000; Dowell *et al*, 1999; Formenti *et al*, 2003; Kao *et al*, 2005).

The adverse effects of radiation, namely, lung toxicities in patients with breast or lung cancer treated by thoracic radiation, are of great concern, and may be dose limiting or even have a negative impact on the quality of life of the patients, even though radiation is an efficient treatment option. Lung toxicities often result in lung fibrosis, necessitating change of the treatment method and causing much distress or even death of the patients (Penney and Rubin, 1977; Early Breast Cancer Trialists' Collaborative Group, 2000; Lind *et al*, 2002). Some clinical trials actually reported an increased incidence of pneumonitis following combined PTX therapy with radiation in patients with breast or lung cancer (Taghian *et al*, 2001; Hanna *et al*, 2002; Chen and Okunieff, 2004).

Although widely used, PTX itself has several adverse effects, such as peripheral sensory neuropathy (Rowinsky *et al*, 1993; Rowinsky and Donehower, 1995), and its poor solubility in water is also associated with such effects as anaphylaxis and other severe hypersensitivity reactions attributable to Cremophor EL and ethanol, which are essential for solubilising PTX (Weiss *et al*, 1990; Rowinsky and Donehower, 1995). In order to overcome these problems, we prepared a new formulation, NK105, which is a PTX-incorporating polymeric micellar nanoparticle (85 nm in size) (Hamaguchi *et al*, 2005). NK105 is formed by facilitating the self-association of amphiphilic block copolymers constructed using polyethylene glycol (PEG) as the hydrophilic segment and modified polyaspartate as the hydrophobic segment in an aqueous medium. Owing to the PEG constituting the outer shell of the micelles, NK105 is soluble in water. In addition, PEG also confers a stealth property to the formulation, that allows the micellar drug preparation to be less avidly taken up by the reticuloendothelial

*Correspondence: Dr Y Matsumura; E-mail: yhmatsum@east.ncc.go.jp
Revised 5 June 2006; accepted 11 July 2006; published online 8 August 2006

system (RES) and to be retained in the circulation for a longer period of time (Klibanov *et al*, 1990, 1991; Allen, 1994; Gabizon *et al*, 1996). The prolonged circulation time and the ability of NK105 to extravasate through the leaky tumour vasculature (i.e., the EPR (enhanced permeability and retention) effect) causes accumulation of PTX in tumour tissues (Matsumura and Maeda, 1986; Maeda and Matsumura, 1989). We previously demonstrated that NK105 is associated with reduced neurotoxicity and also exerts more potent antitumour activity on human cancer xenograft, as compared to free PTX. In addition, because of its solubility in water, it is expected that the incidence of anaphylaxis and hypersensitivity reactions attributable to Cremophor EL and ethanol may also be reduced with NK105. A clinical trial of NK105 is now under way.

In this context, it is expected that the use of NK105 in place of PTX in combination with radiation may also yield superior results, because of the more potent antitumour activity of this drug as compared to that of free PTX. In this study, we evaluated the antitumour activity and severity of lung fibrosis induced by PTX and NK105 administered in combination with thoracic radiation, to examine whether combined NK105 chemotherapy with radiation would be an acceptable or useful treatment modality.

MATERIALS AND METHODS

Mice

Eight-week-old female C57BL/6J mice were purchased from Charles River Japan Inc. (Kanagawa, Japan). All the animal procedures were performed in compliance with the guidelines for the care and use of experimental animals, drawn up by the Committee for Animal Experimentation of the National Cancer Center; these guidelines meet the ethical standards required by law and also comply with the guidelines for the use of experimental animals in Japan.

PTX and NK105

Paclitaxel was purchased from Merican Corp. (Tokyo, Japan). NK105 is a PTX-incorporating 'core-shell-type' polymeric micellar nanoparticle formulation that was prepared by a previously reported procedure (Hamaguchi *et al*, 2005). Briefly, polymeric micellar particles were formed by facilitating the self-association of amphiphilic block copolymers in an aqueous medium. The polymer of NK105 was constructed using PEG as the hydrophilic segment and modified polyaspartate as the hydrophobic segment. The carboxylic groups of the polyaspartate block were modified by the esterification reaction with 4-phenyl-1-butanol, resulting in conversion of half of the groups to 4-phenyl-1-butanolate. Molecular weight of the polymers was determined to be approximately 2000 (PEG block: 12 000; moditied polyaspartate block: 8000).

Via the self-association process, PTX was incorporated into the inner core of the micelle system by physical entrapment through hydrophobic interactions between the drug and specifically well-designed block copolymers for PTX. NK105 was obtained as a freeze-dried formulation and contained ca.23% (WW^{-1}) of PTX. Finally, NK105, PTX-incorporating polymeric micellar nanoparticle formulation with a single and narrow size distribution, was obtained. The weight-average diameter of the nanoparticles was approximately 85 nm ranging from 20 to 430 nm.

Irradiation

The mice were anesthetised by intraperitoneal (i.p.) injection of nembutal (75 mg kg^{-1}) and placed on the stage for irradiation. The whole thorax or subcutaneous (s.c.) tumours of the thigh were irradiated using a Faxitron cabinet X-ray system model CP-160 by 100 kV X-rays from a linear accelerator, at a dose rate of 2 Gy min^{-1}. Totally 12 Gy was irradiated to each mouse. The whole body except irradiated parts, lung field or tumour lesion, were shielded with specially designed lead blocks.

Flow cytometry

At 24 h after the injection of PTX or NK105 into the Lewis lung carcinoma (LLC) tumour-bearing C57BL/6j mice, the tumours were excised, minced in PBS, and fixed in 70% ethanol at 4°C for 48 h. After being fixed, the tumours were digested with 0.04% pepsin (Sigma chemical co., St Louis, MO, USA) in 0.1 N HCl for 60 min at 37°C in a shaking bath for preparing single-nuclei suspensions. The nuclei were then centrifuged, washed twice with PBS, and stained with 40 $\mu g\,ml^{-1}$ of propidium iodide (Molecular Probes, OR, USA) in the presence of 100 $\mu g\,ml^{-1}$ RNase in 1 ml PBS for 30 min at 37°C. The stained nuclei were analysed with a B-D FACSCalibur (BD Biosciences, San Jose, CA, USA). The cell cycle distribution was analysed using the Modfit program (Verity Software House Inc., Topsham, ME, USA).

Evaluation of the antitumour activity

For this experiment, 3×10^6 LLC cells were inoculated s.c. into the right thighs of mice. The tumour volume was calculated using the formula, tumour volume (mm^3) $= a \times b^2/2$ (a = longest tumour diameter, b = shortest tumour diameter). When the tumour volume reached approximately 100 mm^3 on day 14 after the tumour inoculation, the mice were randomly allocated to test groups of about four or five mice each, and started the treatment on the same day. There were six test groups, as follows: untreated control, PTX treatment alone, NK105 treatment alone, radiation alone, combined PTX treatment with radiation, and combined with NK105 treatment with radiation.

In the groups receiving PTX or NK105, the mice were administered a single intravenous (i.v). injection of PTX or NK105 at the dose of 45 mg kg^{-1}; 24 h after the drugs were administered, the tumour sites of the mice in the groups scheduled to receive radiation were irradiated.

The antitumour activity of each treatment regimen was evaluated by measuring the tumour volume. Tumour volume and body weight was measured every 3 days.

Evaluation of lung toxicity

The severity of lung toxicity was evaluated histologically in the following test groups; untreated control ($n=6$), radiation treatment alone ($n=6$), combined PTX treatment with radiation ($n=9$), and combined NK105 treatment with radiation ($n=10$). Mice were administered a single i.v. injection of PTX or NK105 at the dose of 45 mg kg^{-1}; 24 h after the drugs were administered, the thorax of the mice in the groups scheduled to receive radiation was irradiated. All the mice were killed 36 weeks after the drug administration. At the time of the killing, the lungs were removed, and the right lungs were fixed in 10% buffered formalin for 24 h, then embedded in paraffin. The lungs were inflated at 20 cm water pressure by intratracheal infusion of 10% buffered formalin before fixation. Sections (5 μm- thick) were stained with haematoxylin and eosin (H&E) and observed under the light microscope. The severity of the pulmonary fibrosis was assessed based on Ashcroft's scoring system (Ashcroft *et al*, 1988). Briefly, all the fields of each lung section were scanned under a Leica microscope at a magnification of $\times$ 100, then each field was visually graded from 0 (normal lung) to 8 (total fibrotic obliteration of the field). The mean grades obtained for all of the fields was then calculated as the visual fibrotic score.